Pacific Northwest
NATIONAL LABORATORY

PNNL-37627 Rev 0
ITSW-RPT-005 Rev 0

FY24 Task 5: Leachate Disposition

April 2025

Amy M Westesen
Susan E Asmussen
Austin A Bachman
Truc Trang-Le
Luke Sweet
Edgar C Buck
Reid A Peterson

U.S. DEPARTMENT OF ENERGY

Prepared for the U.S. Department of Energy
under Contract DE-AC05-76RL01830

DISCLAIMER

PACIFIC NORTHWEST NATIONAL LABORATORY
operated by
BATTELLE
for the
UNITED STATES DEPARTMENT OF ENERGY
under Contract DE-AC05-76RL01830

Printed in the United States of America

Available to DOE and DOE contractors from
the Office of Scientific and Technical Information,
P.O. Box 62, Oak Ridge, TN 37831-0062
www.osti.gov
ph: (865) 576-8401
fax: (865) 576-5728
email: reports@osti.gov

Available to the public from the National Technical Information Service
5301 Shawnee Rd., Alexandria, VA 22312
ph: (800) 553-NTIS (6847)
or (703) 605-6000
email: info@ntis.gov
Online ordering: http://www.ntis.gov

PNNL-37627 Rev 0
ITSW-RPT-005 Rev 0

FY24 Task 5: Leachate Disposition

April 2025

Amy M Westesen
Susan E Asmussen
Austin A Bachman
Truc Trang-Le
Luke Sweet
Edgar C Buck
Reid A Peterson

Prepared for
the U.S. Department of Energy
under Contract DE-AC05-76RL01830

Pacific Northwest National Laboratory
Richland, Washington 99354

Contents

Figures

Tables

Acknowledgements

The authors thank Dr. Ming Zhu (DOE-EM) for supporting this work. Pacific Northwest National Laboratory (PNNL) is operated by Battelle for the U.S. Department of Energy under the contract DE-AC05-76RL01830. The authors thank Heather Colburn and Renee Russell for conducting the technical reviews of the calculation files and this report. The authors also thank David MacPherson for the quality review of the calculation files and this report as well as Matt Wilburn for his technical editing contribution to this report.

1.0 Introduction

Directly feeding sludge solids to the high-level waste (HLW) Waste Treatment Plant Vitrification Facility represents an alternative flowsheet seeking to initiate sludge processing as soon as possible. Key processing functions previously captured during baseline pretreatment operations include leaching and washing prior to solids concentration. These operations should be considered in the potential direct feed flowsheets to maximize waste feed loading, minimize HLW volume, and mitigate corrosion challenges associated with vitrification of high phosphate and fluoride concentrations. Additionally, single-shell tank (SST) retrievals and waste transfers to double-shell tanks (DSTs) in a direct feed flowsheet would likely also benefit from some level of leaching, washing, and solids concentration in order to reduce DST space and mission duration. These operations could occur in a new facility or potentially in available DSTs. If washing and leaching are utilized, an effective disposition pathway for the wash water and leachate solutions are needed. This Task 5 report details the testing executed in fiscal year (FY) 2024 in order to assess potential leachate disposition pathways.

Three target species that benefit significantly from leaching and washing are phosphate, fluoride and aluminum. Phosphate (PO_4^{3-}) and fluoride (F^-) can contribute substantially to the amount of carrier fluid needed for dissolution, and the resulting volume of liquid generated. Disposition of this retrieval solution should be evaluated in order to prevent crystallization of these anions throughout system processing. Since there is a high probability that any retrieval solutions will be at or near their PO_4^{3-} and F^- solubility limits, evaporation or blending with a high Na supernate (>3.5 M) is not recommended for the wash water streams without a method to remove precipitants prior to solution disposal. Additionally, aluminum present in the southeast quadrant of the Hanford site represents roughly 60% of the waste solids in the initial processing tanks. These aluminum solids are in the form of gibbsite ($Al(OH)_3$) and can pose significant challenges for processing due to the fast-settling times and high solids loading associated with these materials. Easily remediated by caustic addition to the solids, these wash solutions could be processed through crystalline silicotitanate (CST) ion exchange columns to prepare the supernate solutions for disposition.

The current target for feed conditions to the Low Activity Waste (LAW) melter are waste streams that contain nominally 5-6 M Na. Fractions within the tanks contain upwards of 0.2 M phosphate and fluoride in solution at 3.5 M Na. Concentrating these solutions above 5 M Na would result in an exceedance of the solubility limits, and potential for uncontrolled precipitation of the phosphate and fluoride crystal material. The resulting crystalline salt material is typically sodium fluoride phosphate, also referred to as natrophosphate ($Na_7FPO_4 \cdot 19H_2O$). Salt phases are of importance in tank waste due to their chemical reactivity, which can result in precipitation, dissolution, or transformation, impacting any downstream processes (Bolling et al. 2020, Russell, Snow, and Peterson 2010). Salt generation and precipitation could pose challenges by causing system plugging and melter corrosion if left in the supernate stream, or limit sodium molarity of the supernate that would be accepted without incident in waste operations.

To understand the impact of this salt generation, the crystallization of natrophosphate in multiple simulant feed matrices was studied to understand the implications of various tank waste supernate chemistries. Three matrices were examined: high PO_4^{3-}/low F^-, low PO_4^{3-}/high F^-, and an average matrix. Subsequent testing was performed with the average matrix with the inclusion of $CsNO_3$, and a final run with the average matrix including $CsNO_3$ and a ^{137}Cs spike for tracer purposes.

2.0 Quality Assurance

This work was performed in accordance with the Pacific Northwest National Laboratory (PNNL) Nuclear Quality Assurance Program (NQAP). The NQAP complies with the United States Department of Energy Order 414.1D, *Quality Assurance,* and 10 CFR 830, Subpart A, *Quality Assurance Requirements*. The NQAP uses NQA-1-2012, *Quality Assurance Requirements for Nuclear Facility Applications,* as its consensus standard and NQA-1-2012, Subpart 4.2.1, as the basis for its graded approach to quality.

The NQAP works in conjunction with PNNL's laboratory-level Quality Management Program, which is based upon the requirements as defined in the United States Department of Energy (DOE) Order 414.1D, *Quality Assurance,* and 10 CFR 830, Subpart A, *Quality Assurance Requirements*.

3.0 Test Conditions

This section describes the simulant formulation and preparation, CST media, column and batch contact ion exchange conditions, evaporation conditions, and sample analysis. All testing was conducted in accordance with a task plan prepared by Pacific Northwest National Laboratory (PNNL) and approved by Department of Energy Headquarters (DOE HQ). [1]

3.1 Simulant Formulation and Preparation

Sample evaluation from core segments in tanks AN-101 and AN-106 with high gibbsite ($Al(OH)_3$) and high natrophosphate ($Na_7(PO_4)_2F•19H_2O$) layers determined the concentrations targeted for the prepared simulants reported herein. Figure 3.1 shows the sludge segment chemistry from Hanford's Best Basis Inventory (BBI) converted into wt% for AN-101 (top) and AN-106 (bottom). Segments of concern for aluminum are 18LH for AN-101 and 14, 15UH, 15LH, and 16UH for AN-106 as they all contain (>70 wt% gibbsite). The average supernate chemistry associated with these core segments was used as a baseline for the high aluminum leachate solution. Table 3.1 shows the supernate concentration of the segment layers alongside the target simulant matrix concentration used in this testing. Supernate concentrations were all normalized to 5.5 M Na to mimic a prepared matrix currently acceptable for tank side cesium removal (TSCR) (between 5-6 M Na).

High natrophosphate concentrations of concern are found in AN-101 segments 13LH and 19LH, and AN-106 segments 16LH, 19UH, and 20UH due to substantial amounts (>30 wt%) of natrophosphate layers. Table 3.2 shows the current supernate concentration of the specified segment layers. These concentrations were normalized to Na and averaged to target a simulant makeup between 0.5 and 3.8 M Na, shown in Table 3.3. These matrices were selected to bound potential wash operations ranging from water addition needed to dissolve maximum amounts of PO_4^{3-} and F^- (0.5 M Na) to the minimum needed to maintain a 1.20 g/mL density required for sludge transport (3.8 M Na).

[1]Westesen AM. 2024. Task Plan ITSW-TP-001, Rev. 0.0. *In Tank Treatment Task 5- Leachate and Wash Water Disposition (FY24).* Pacific Northwest National Laboratory, Richland, Washington. Not publicly available.

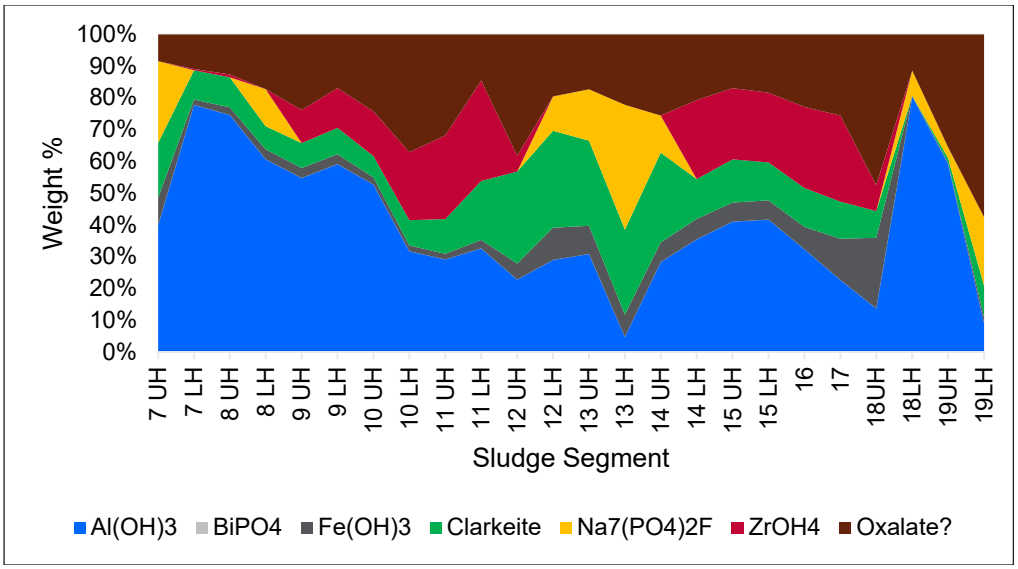

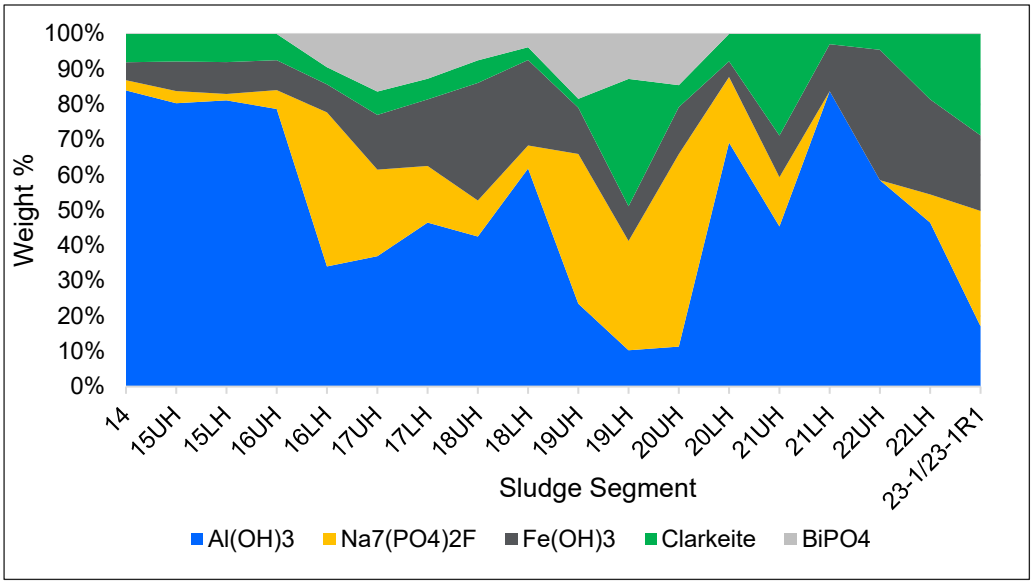

Figure 3.1. Tank AN-101 (top) and AN-106 (bottom) Sludge Segments

Table 3.1 Aluminum Supernate and Simulant Composition

Component	AN-101 18LH[a], M	AN-106 14[b], M	AN-106 15UH[b], M	AN-106 15LH[b], M	AN-106 16UH[b], M	Target Simulant Concentration, M
Fluoride	0.003	0.08	0.15	0.16	0.15	0.13
Phosphate	0.03	0.01	0.03	0.03	0.03	0.03
Sodium	7.78	5.78	3.47	3.59	3.75	5.50
Nitrite	2.28	1.09	0.75	0.80	0.93	1.00
Nitrate	2.63	0.87	0.29	0.38	0.65	1.69
Hydroxide	1.67	1.95	0.96	0.82	0.84	1.05
TIC (carbonate)	0.57	0.59	0.55	0.54	0.53	0.50
Aluminum	0.34	0.36	0.14	0.15	0.16	0.55
Potassium	0.10	0.05	0.02	0.02	0.02	0.04

[a] RPP-RPT-63675-00-Record
[b] RPP-RPT-63779-00-Record

Table 3.2 Average PO_4^{3-}/F^- Supernate Composition

Component	AN-101 13LH[a], M	AN-101 19LH[a], M	AN-106 16UH[b], M	AN-106 19UH[b], M	AN-106 20UH[b], M
Fluoride	0.13	0.08	0.16	0.04	0.02
Phosphate	0.02	0.02	0.02	0.17	0.15
Sodium	5.96	7.22	3.80	3.10	3.06
Nitrite	1.38	1.95	0.88	0.86	0.74
Nitrate	1.34	2.15	0.66	0.29	0.23
Hydroxide	0.68	1.38	0.10	0.02	0.10
TIC (carbonate)	0.97	0.25	0.48	0.68	0.66
Aluminum	0.15	0.30	0.20	0.01	0.01
Potassium	0.07	0.09	0.03	0.02	0.03

[a] RPP-RPT-63675-00-Record
[b] RPP-RPT-63779-00-Record

Table 3.3 Average PO_4^{3-}/F^- Simulant Composition

Component	0.5 M Na Simulant, M	1.0 M Na Simulant, M	2.0 M Na Simulant, M	3.0 M Na Simulant, M	3.8 M Na Simulant, M
Fluoride	0.01	0.02	0.04	0.06	0.07
Phosphate	0.01	0.02	0.05	0.07	0.09
Sodium	0.50	1.00	2.00	3.00	3.80
Nitrite	0.14	0.28	0.56	0.84	1.06
Nitrate	0.09	0.19	0.37	0.56	0.71
Hydroxide	0.04	0.08	0.15	0.23	0.29
TIC (carbonate)	0.09	0.17	0.34	0.52	0.65
Aluminum	0.01	0.02	0.05	0.07	0.09
Potassium	0.005	0.01	0.02	0.03	0.03

The equilibrium solubility of natrophosphate determines the maximum amount of fluoride and phosphate that can be present in the solution. Figure 3.2 shows the directly observable solubility for experimental data in a 3.5 M Na solution (Westesen et al. 2023).

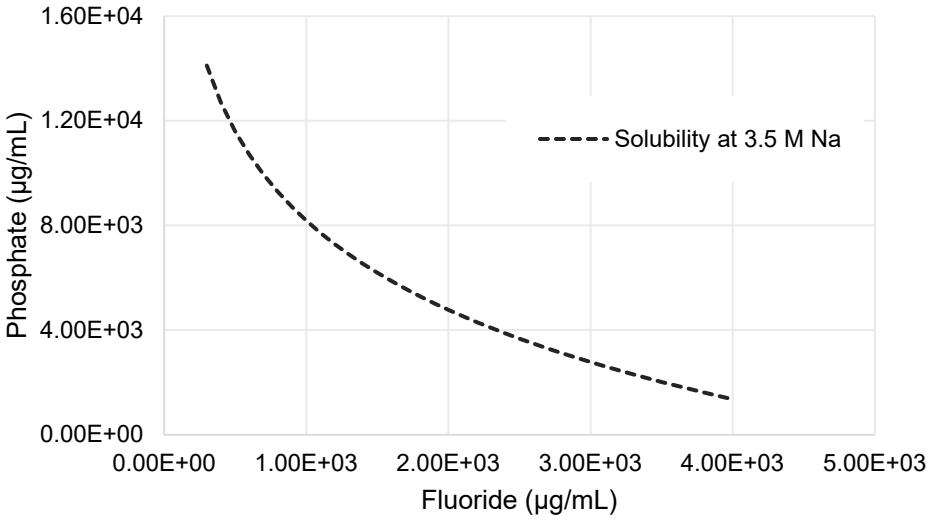

Figure 3.2. Phosphate and Fluoride Solubility

Given this inverse relationship in solubility between PO_4^{3-} and F^-, two additional simulants (shown in Table 3.4) were prepared at the high PO_4^{3-}/low F^- and low PO_4^{3-}/high F^- fractions to mimic the tank conditions seen in AN-106 segments 16UH and 19LH.

Table 3.4 High PO4/Low F and Low PO4/High F Simulant Composition

Component	High Phosphate/Low Fluoride Simulant, M	Low Phosphate/High Fluoride Simulant, M
Fluoride	0.070	0.200
Phosphate	0.200	0.090
Sodium	3.80	3.80
Nitrite	1.060	1.060
Nitrate	0.390	0.590
Hydroxide	0.290	0.290
TIC (carbonate)	0.650	0.650
Aluminum	0.090	0.090
Potassium	0.030	0.030

All simulants were prepared from ACS reagent grade materials shown in Table 3.5.Component masses were measured into volumetric flasks containing part of the requisite deionized (DI) water. After all salts were added and dissolved, the solution was brought to volume with DI water. All densities were measured in the preparation volumetric flask at room temperature, ~20 °C. Each solution was passed through a 0.45-micron pore size nylon filter 24 h after preparation to remove any precipitated components. The densities were remeasured and agreed with the pre-filtered solution density within expected uncertainty.

Table 3.5 Reagents used for Simulant Preparation

Compound	MW, g/mole	Manufacturer	Lot Number
50% NaOH	40.00	Sigma-Aldrich	4102497307
$Al(NO_3)_3•9H_2O$	375.13	Sigma-Aldrich	BCBR0256V
$CsNO_3$	194.91	Aldrich	MKBS6216V
KCl	74.55	Sigma-Aldrich	SLBR2609V
KF	58.09	Thiokol Ventron	020180
$NaAlO_2$	81.97	Sigma-Aldrich	102667009
NaF	41.99	Sigma-Aldrich	MKCV4470
$NaNO_2$	69.00	Sigma-Aldrich	MKBV1410V
$NaNO_3$	84.99	Sigma-Aldrich	BCBK9624V
Na_3PO_4-$12H_2O$	380.12	Fisher	126469
Na_2CO_3	105.98	Sigma-Aldrich	1003143649

Table 3.6 provides the calculated and measured component concentrations for the 5.5 M Na Aluminum Simulant and the 3.8 M Na Avg PO_4/F, High PO_4/Low F, and Low PO_4/High F

Simulants. A sample of each simulant was submitted for anion analysis by ion chromatography (IC) (F^-, Cl^-, NO_2^-, NO_3^-, and PO_4^{3-}), carbon analysis by hot persulfate oxidation (TOC/Total Carbon), and Al, Na, and K analysis by inductively coupled plasma optical emission spectroscopy (ICP-OES). The calculated concentrations for all components except phosphate were considered definitive. Because loss of phosphate due to solubility restrictions was possible during simulant preparation, the measured concentrations were expected to be the definitive values. The 3.8 M Na Avg PO_4/F simulant underwent serial dilutions with DI water to prepare the 3.0, 2.0, 1.0 and 0.5 M Na solutions.

Table 3.6 Calculated and Measured Simulant Compositions

Simulant>>	Al Simulant		Avg PO_4/F Simulant		High PO_4/Low F Simulant		Low PO_4/High F Simulant	
Ion	Calculated Molarity	Measured Molarity	Calculated Molarity	Measured Molarity	Calculated Molarity	Measured Molarity	Calculated Molarity	Measured Molarity
Al^+	0.55	0.511	0.09	0.090	0.09	0.087	0.09	0.086
OH^-	1.05	NM	0.29	NM	0.29	NM	0.29	NM
F^-	0.13	0.094	0.07	0.055	0.07	0.022	0.20	0.174
Cl^-	0.03	0.032	0.03	0.032	0.03	0.027	0.03	0.027
K^+	0.03	0.042	0.03	0.044	0.03	0.031	0.03	0.031
NO_2^-	0.99	1.013	1.06	1.067	1.06	1.048	1.06	1.061
NO_3^-	1.69	1.629	0.71	0.676	0.39	0.389	0.59	0.582
PO_4^{3-}	0.03	0.016	0.09	0.048	0.20	0.100	0.09	0.031
CO_3^{2-}	0.50	0.513	0.65	0.614	0.65	0.514	0.65	0.551
Na^+	5.49	5.350	3.80	3.590	3.80	3.071	3.80	3.093

3.2 CST Media

The CST used in this testing was procured by Hanford Tank Waste Operations and Closure (H2C formally known as Washington River Protection Solutions) as ten 5-gallon buckets (149 kg total) of IONSIV R9140-B, lot number 2002009604, from Honeywell UOP, LLC. The CST was transferred to PNNL for use in laboratory testing described herein. Details of the procurement and material properties can be found elsewhere (Fiskum et al. 2019a). Before use in column and batch contact testing, the CST was sieved to <30-mesh and pretreated by contacting with 0.1 M NaOH successively until fines were no longer observed. The <30-mesh CST sieve cut has been shown to provide appropriate performance scaling to a full-height TSCR column (Westesen et al. 2020).

3.3 Ion Exchange Column Operations

Ion exchange column operations were conducted with the 5.5 M Na high aluminum simulant. Historically, there has been some experience with CST plugging with certain high aluminum bearing streams (Wilmarth et al. 2000) so an assessment of a leachate prototypic of SE area sludge was conducted to determine the ion exchange processing performance. The ion exchange system was set up as shown schematically in Figure 3.3 (lead to lag solution flow). The system consisted of two columns containing CST ion exchange media, a small metering

pump, three valves, a pressure gauge, and a pressure-relief valve. The valves were three-way valves that could be turned to the flow position (upward) to flow solution through the entire system or a sample position (downward) to collect samples/fluids. Valve 1 was placed near the outlet of the pump and was used to isolate the column from the pump, to collect initial fluids and to expel air from the lines at the initial setup. Valves 2 and 3 were primarily used to obtain samples and closed to isolate the system during storage periods.

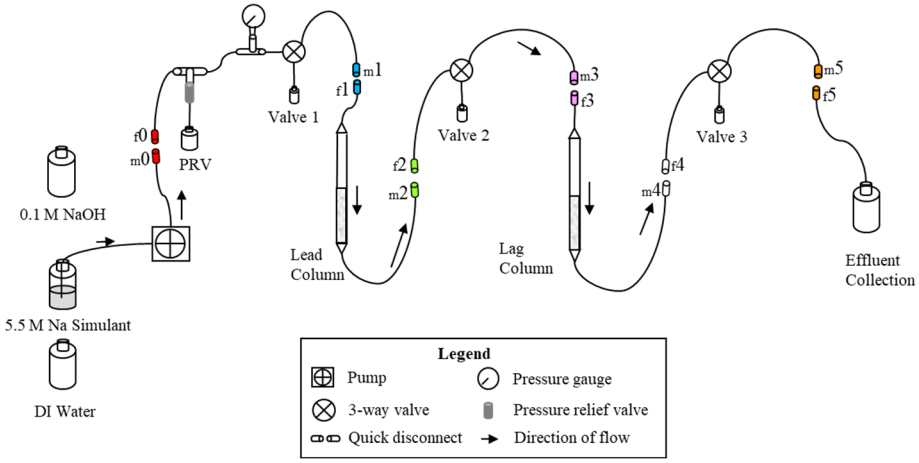

Figure 3.3. Ion Exchange System Schematic

Chromaflex column assemblies made of borosilicate glass 9 cm tall with an inside diameter of 1.5 cm were used. The CST was supported by an in-house-constructed support consisting of a 200-mesh stainless steel screen tack welded onto a stainless-steel O-ring. The flared cavity at the bottom of each column was filled to the extent possible with 4-mm-diameter glass beads to minimize the mixing volume below the CST bed. An adhesive centimeter scale with 1-mm divisions (Oregon Rule Co., Oregon City, OR) was affixed to each column with the 0-point coincident with the top of the support screen.

Aliquots of settled CST (pretreated, <30 mesh) were measured using a graduated cylinder and then quantitatively transferred to each individual column. Testing used 6.0-mL CST in each column. The CST was allowed to settle through a 0.1 M NaOH solution to mitigate any gas bubble entrainment. The columns were tapped with a rubber bung until the CST height no longer changed. The CST bed volume (BV) corresponded to the settled CST media volume as measured in the graduated cylinder prior to transferring the media into the ion exchange column.

Four liters of the 5.5 M Na Al simulant was prepared to use in the column testing. The simulant was spiked with a $CsNO_3$ tracer to a nominal 9.37 µg/mL (6.99E-05 M) Cs concentration based on supernate characterization from the AN-101 and AN-106 tanks. Radioactive ^{137}Cs was also added to the simulant feed to count the processing samples by Gamma Energy Analysis (GEA). Feed was processed at 1.9 BVs per hour. The flowrate, in terms of contact time with the CST bed, matched the expected flowrate at TSCR.

After the 5.5 M Na Al simulant processing (also “loading” in subsequent discussion) was completed, ~12 BVs (2 mL) of 0.1 M NaOH feed displacement (FD) followed by ~12 BVs of DI water were passed downflow through the system to rinse residual feed out of the columns and process lines.

Figure 3.4 provides daily temperature and flowrate profiles of the aluminum simulant processing as it went through the columns. Temperature was measured using a thermocouple placed inside a vial of water within the fume hood. The system temperature averaged 20.2 °C throughout the testing, with a variance of temperatures from 17.9 to 22.8 °C. The pump head stroke length was close to the minimum at which it could be set. The stroke rate was adjusted throughout testing to maintain the flowrate between 1.7 and 2.2 BV/h. Test parameters, including process volumes, flowrates, and CST contact times, are summarized in Table 3.7.

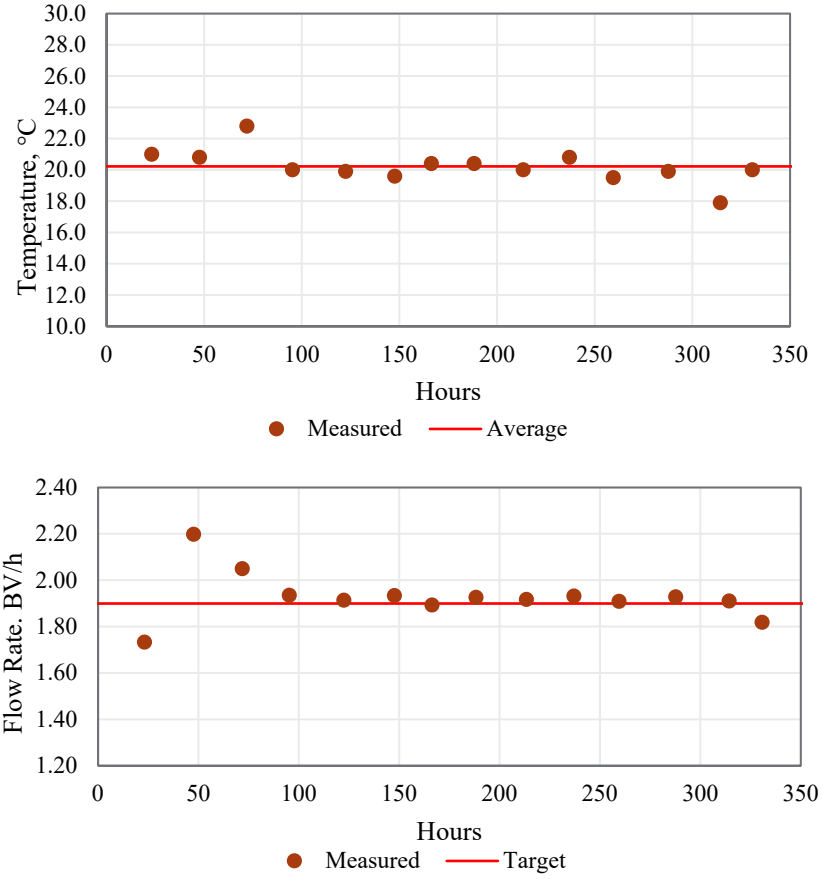

Figure 3.4 Al Simulant Daily Column Temperature and Flowrate during Testing

Table 3.7 Experimental Conditions for Al Simulant Column Processing

Process Step	Solution	Volume		Flowrate		Duration
		(BV)	(mL)	(BV/h)	(mL/min)	(h)
Lead and Lag Column Loading	5.5 M Na Al Simulant	637.0	3822	1.93	0.193	336:23
Feed displacement	0.1 M NaOH	11.2	67.5	2.67	0.267	4:13
Water rinse	DI water	13.5	81.2	2.66	0.266	5:05
Flush with compressed air	NA	4.7	28.4	NA	NA	NA

BV = bed volume (6.0 mL as measured in graduated cylinder).
DI = deionized.
NA = not applicable.

The total cumulative volume of 5.5 M Na Al simulant processed was 3.8 L (637 BVs). The process cycle mimicked, as best as possible, the process flow to be experienced at the TSCR facility in terms of Na concentration, BV/h (i.e., contact time), FD, and water rinse. It was understood that the feed linear flow velocity in this small-column configuration (0.109 cm/min) could not begin to match that of the full-height processing configuration (7.3 cm/min, Fiskum et al. 2019a). The objective was to match contact time in the bed.

During the loading phase, nominal 2-mL samples were collected from the lead and lag columns at the sample collection ports (see Figure 3.3, valves 2 and 3). Sampling from the columns necessitated brief (~15-min) interruptions of flow to the downstream columns. Samples were collected after the first 10 BVs were processed and again at nominal 25- to 100-BV increments. Only brief (~3-min) interruptions were associated with changing the feed bottles.

The FD and water rinse effluents were collected in bulk in a 125-mL polyethylene bottle. The fluid-filled volume was expelled with compressed air in ~8 min. The collected volume (28 mL) did include the interstitial fluid space between the CST beads but was not expected to include fluid in the CST pore space. Hours of additional gas flow were required to dry the CST enough to be free flowing.

3.4 Batch Contact Conditions

Batch contact testing to assess the effect of caustic sludge leachate on the CST exchange functionality and capacity for Cs was determined on four different PO_4/F simulants. Initial tests were performed with the PO_4/F simulant matrices from Table 3.6. The Avg PO_4/F 3.8 M Na simulant was additionally diluted down to test conditions at 3.0, 2.0, 1.0 and 0.5 M Na to investigate the impact of Na concentration on Cs removal. Calculated volumes of the prepared 3.8 M Na simulant were divided and individually diluted with the appropriate volume of DI water to generate 125-mL of each target Na solution. The volumes were transferred via volumetric pipet and the net mass of solution was recorded. The measured density of the prepared 3.8 M Na simulant was used to confirm volume ratios and targeted Na concentrations.

The High PO4/Low F and Low PO4/High F matrices determined the specific impacts from varying the PO_4 and F anion concentrations. An additional simulant was prepared at 1.9 M Na and included higher concentrations of PO4 and F than the average PO_4/F simulant diluted down to 2.0 M Na to mimic the additional solubility of those anions at a lower Na concentration. The composition of the 1.9 M Na washed simulant is shown in Table 3.8.

Table 3.8 1.9 M Na Washed PO4/F Simulant

Component	1.9 M Na Washed PO4/F Simulant, M
Fluoride	0.150
Phosphate	0.150
Sodium	1.90
Nitrite	0.370
Nitrate	0.270
Hydroxide	0.110
TIC (carbonate)	0.250
Aluminum	0.050
Potassium	0.020

Aliquots (125-mL) of each simulant were spiked with $CsNO_3$ to achieve Cs concentrations of 3.3E-5, 1.3E-4, 7.8E-4, and 1.5E-2 M Cs. Each simulant was spiked with a ^{137}Cs tracer to achieve a concentration of ~0.1 µCi/mL; a 2-mL aliquot of each spiked simulant was collected for GEA; this value served as the baseline (C_0) ^{137}Cs concentration.

Nominal 0.075-g (dry mass basis) aliquots of CST were measured into 20-mL vials. F-factor samples were collected in duplicate, bracketing batch contact aliquots, and used to determine the dry mass of the exchanger. The F-factor was measured at 105 °C with an average value of 0.934. The F-factor at 105 °C measured at the time of the experiment was used to calculate the dry mass of CST for each of the simulant batch contact tests.

A 15-mL aliquot of each simulant solution was added to the CST aliquot; exact volume was determined from net solution mass and density. The solution volume-to-CST mass phase ratios averaged 198 (range 186 to 203). Samples were mixed for 140 h at 25 °C on a Cole-Parmer (Vernon Hills, Illinois) large orbital shaker with a 16-mm orbit set to 240 rpm. A vial of water was co-located with the sample set to serve as a temperature sentinel; its temperature was measured periodically during the contact period with a type K thermocouple (measurement uncertainty of ±2.2 °C). After the contact time was completed, the samples were removed and then phase separated by filtration through a 0.45-micron pore size nylon syringe filter. The ^{137}Cs concentration (C_1) was measured in the post-contacted solutions using GEA, and the measured ^{137}Cs tracer fractionation was used to determine the total Cs exchange. The isotherm data were fitted to a Freundlich/Langmuir hybrid equilibrium fit (Hamm et al. 2002).

The batch distribution coefficients were calculated according to Eq (3.1).

$$\frac{(A_0 - A_1)}{A_1} \times \frac{V}{M \times F} = K_d \qquad (3.1)$$

where A_0 = initial ^{137}Cs concentration (µCi/mL)
A_1 = final (equilibrium) ^{137}Cs concentration (µCi/mL)
V = volume of the batch contact liquid (mL)
M = measured mass of CST (g)
F = F-factor, mass of the 105 °C dried CST divided by the mass of the undried CST
K_d = batch-distribution coefficient (mL/g)

Final (equilibrium) Cs concentrations (C_{Eq}) were calculated relative to the tracer recovered in the contacted samples (A_1) and the initial metal concentration (C_0) according to Eq. (3.2)

$$C_0 \times \left(\frac{A_1}{A_0}\right) = C_{Eq} \qquad (3.2)$$

where C_0 = initial Cs concentration in solution (µg/mL or M)
C_{Eq} = equilibrium Cs concentration in solution (µg/mL or M)

The equilibrium Cs concentrations loaded onto the CST (Q in units of mmoles Cs per gram of dry CST mass) were calculated according to Eq. (3.3)

$$\frac{C_0 \times V \times \left(1 - \frac{A_1}{A_0}\right)}{M \times F \times 1000 \times FW} = Q \qquad (3.3)$$

where Q = equilibrium Cs concentration in the CST (mmole/g CST)
1000 = conversion factor to convert µg to mg
FW = Cs formula weight

3.5 Evaporation and Crystallization

3.5.1 Simulant Matrices and Preparation

The evaporation and subsequent crystallization of simulants was studied on three simulant matrices with varying fluoride and phosphate concentrations to assess any impact on natrophosphate precipitation. The simulant test matrix was modeled to represent the AN-101 and AN-106 supernate segments at high (>30 wt%) natrophosphate ($Na_7FPO_4 \cdot 19H_2O$) as described in Section 3.1. Simulants were normalized to 3.8 M Na for ionic strength. To account for the inverse solubility relationship between PO_4^{3-} and F^- (Section 3.1, Figure 3.2) an average simulant, and both high PO_4^{3-}/low F^- and low PO_4^{3-}/high F^- simulants were developed. While the average simulant matrix composition considered the multiple segments from AN-101 and AN-106, the high PO_4^{3-}/low F^- simulant modeled the AN-101 13LH supernate concentration due to the high phosphate content observed, while the low PO_4^{3-}/high F^- simulant was closely modeled to the AN-106 20UH segment.

Two further variations of the average simulant were also tested with the addition of Cs to the matrix to trace the component through the evaporation process: one simulant included non-radiological $CsNO_3$ (Cs-133), and a second included both non-radiological $CsNO_3$ and a radiological Cs-137 spike. The composition of all matrices is presented in Table 3.9.

Table 3.9. Simulant matrices for evaporation.

Component	Average Simulant Target Concentration, M	High F^-/Low PO_4^{3-} Target Concentration, M	Low F^-/High PO_4^{3-} Simulant Concentration, M	Average Simulant with $CsNO_3$ Target Concentration, M
Fluoride	0.072	0.086	0.026	0.072
Phosphate	0.088	0.011	0.181	0.088
Sodium	3.80	3.80	3.80	3.80
Nitrite	1.065	0.928	0.985	1.065
Nitrate	0.709	0.899	0.288	0.709
Hydroxide	0.281	0.435	0.122	0.281
TIC (carbonate)	0.658	0.663	0.912	0.658
Aluminum	0.094	0.094	0.012	0.094
Potassium	0.034	0.041	0.033	0.034
Cesium	--	--	--	4.36E-04

Simulant preparation was completed with ACS reagent grade materials with the molecular weights listed in Table 3.10. Preparation of the simulant followed the process as described in Section 3.1. To promote the dissolution of chemical components in the solution, some were heated at low heat while stirring.

Table 3.10 Simulant Reagent Materials

Compound	Molecular Weight, g/mol	Manufacturer	Lot Number
$NaAlO_2$	81.97	Sigma-Aldrich	STBL1286
50% NaOH	40.00	Sigma-Aldrich	MKCQ3131
NaF	41.99	Sigma-Aldrich	MKCM8713
KCl	74.55	Sigma	SLBR2609V
$NaNO_2$	69.00	Sigma-Aldrich	MKCT7654
$NaNO_3$	84.99	Thermo Scientific	X05I044
Na_3PO_4-$12H_2O$	380.12	Sigma-Aldrich	MKCS0002
Na_2CO_3	105.99	Sigma-Aldrich	MKCT1777
$CsNO_3$	194.91	Aldrich	MKBS6216V

The density of the simulants was measured following filtration through a 0.45-micron pore size nylon filter after settling for a minimum of 24 h. Simulant composition was determined via IC for F^-, Cl^-, NO_2^-, NO_3^-, and PO_4^3, ICP-OES for Al^+, Na^+, and K^+ analysis, and carbon analysis through hot persulfate oxidation. Calculated concentrations are presented in conjunction with measured analytical concentrations in Table 3.11. The differences between the expected and measured concentrations were likely driven by precipitation of limited dissolution during fabrication (e.g., Al^+, F^-, CO_3^{2-}). The pH of the simulants was 13.

Table 3.11 Calculated and Measured Simulant Compositions for Evaporation

Simulant	Average PO_4^{3-}/F^- Simulant		High PO_4^{3-}/Low F^- Simulant		Low PO_4^{3-}/High F^- Simulant		Average PO_4^{3-}/F^- with $CsNO_3$ Simulant		Average PO_4^{3-}/F^- with $CsNO_3$ and ^{137}Cs Simulant	
Density, g/mL	1.18		1.18		1.17		1.18		1.18	
Ion	Calcd. Conc., mol/L	Meas. Conc., mol/L	Calcd. Conc., mol/L	Meas. Conc., mol/L	Calcd. Conc., mol/L	Meas. Conc., mol/L	Calcd. Conc., mol/L	Meas. Conc., mol/L	Calcd. Conc., mol/L	Meas. Conc., mol/L
Al^+	0.094	0.064	0.012	0.012	0.094	0.098	0.094	0.090	0.094	0.077
OH^-	0.281	--	0.122	--	0.433	--	0.281	--	0.281	--
F^-	0.073	0.051	0.026	0.012	0.086	0.090	0.072	0.052	0.072	0.052
Cl^-	0.035	0.034	0.033	0.028	0.041	0.038	0.034	0.032	0.034	0.032
K^+	0.035	0.032	0.033	0.040	0.041	0.048	0.034	0.034	0.034	0.032
NO_2^-	1.060	1.072	0.990	0.965	0.928	0.959	1.069	1.063	1.067	1.061
NO_3^-	0.712	0.706	0.288	0.266	0.898	0.874	0.710	0.708	0.710	0.706
PO_4^{3-}	0.088	0.054	0.182	0.123	0.011	0.008	0.088	0.053	0.088	0.053
CO_3^{2-}	0.660	0.110	0.916	0.182	0.663	0.128	0.657	0.111	0.658	0.110
Na^+	3.80	3.56	3.82	3.57	3.80	3.70	3.80	3.85	3.80	3.45
Cs^+	N/A	N/A	N/A	N/A	N/A	N/A	4.36E-04	3.69E-04§	4.36E-04‡	--

-- Indicates that the analytical result was not measured.
Analytes not included in the simulant matrix are marked as N/A.
§Cs-133 mass calculated through ICP-MS.
‡Cs-137 mass calculated through GEA.

3.5.2 Evaporation Operations

Evaporation with resulting crystallization was performed with all simulant matrices. The evaporation system was set up as schematically illustrated in Figure 3.5, and shown partially in Figure 3.6. The system consisted of a heating mantle seated on a stir plate (optional) or lab jack that contained the evaporation reaction vessel. The heating mantle was used to provide uniform heating through the reaction vessel. The reaction vessel was a 2-L cylindrical, heavy wall reaction flask that clamped to a head with four inline necks for sample port and attachments. Attached to the evaporation vessel was a condenser that was utilized with a chiller to off-gas condensate collection in the evaporator condensate flask. A vacuum pump was used in all experimental iterations to simulate prototypic operations. The temperature of the evaporator reaction vessel was monitored throughout the process and a dual thermocouple provided overtemperature control. The target temperature for the prototypic operations was ideally 60°C, but the actual boiling point was dependent on the vacuum achieved in the system, and was typically closer to 80°C.

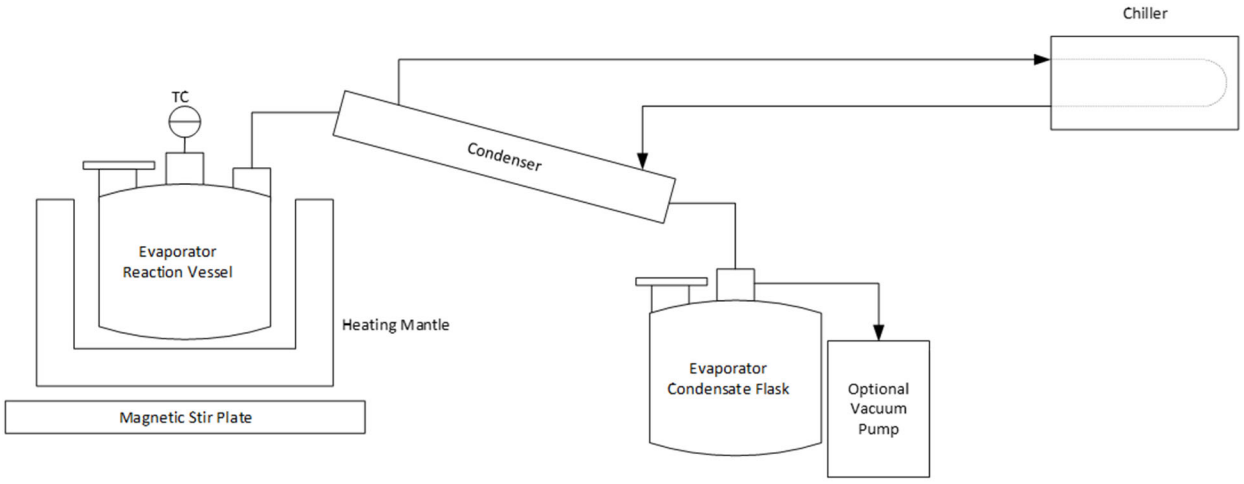

Figure 3.5 Schematic of the Evaporation System

Figure 3.6 Non-Radiological Set Up of Evaporation System (vacuum and chiller not attached; optional lab jack is utilized here).

For each of the five simulant matrices, 2-L of simulant was prepared. The fifth simulant, which included $CsNO_3$ and ^{137}Cs, was spiked with 50 µL of a ^{137}Cs stock tracer, resulting in a concentration of 3.6×10^{-7} M ^{137}Cs to analyze resulting post-evaporate phases by GEA.

When the system was operated, simulant was added to the evaporator reaction vessel via funnel. Once the system was sealed with appropriate plugs to facilitate thermocouple readings and equipment connections, the chiller (attached to the condenser) was turned on, followed by the vacuum and the heating mantle. The system was gradually brought to a low boil under the applied vacuum, which typically occurred around 80 °C. The non-radiological evaporation runs (those without the addition of the ^{137}Cs spike for tracer purposes) nominally observed 19 in Hg (9.33 psi) through the duration of the experiment. The radiological run with ^{137}Cs tracer did not have a read out of the vacuum pulled on the system, however, the specifications of the vacuums were similar, and with the identical system, it can be extrapolated that the vacuum pulled on the system was nominally equivalent.

The evaporation process was monitored by simulant volume in the evaporator reaction vessel and off-gas condensate collection in the evaporator condensate flask for progress and completeness. The final concentration target in the evaporated simulant was 5.6 M Na in all experiments, or a final volume of 1.36 L; volume markings on glassware were used to monitor and indicate experiment completeness. Due to the nature of the pump, it was anticipated that the volume observation would only provide an estimate, as the pump does consume some of the off-gas condensate generated. Estimates of system loss were calculated for each run (~ 100 mL of liquid lost, except for the run with ^{137}Cs).

Upon completion of the experiment, per visual observation of the collected off-gas condensate volume and remaining simulant volume, the vacuum system was halted, the chiller turned off, and the system was allowed to cool while adjusting to normal atmospheric pressure. The system was then allowed to settle for a minimum of 24 h to allow for the generation and precipitation of crystal salt material in the liquid phases.

A vacuum filtration system was employed to filter the crystalline material precipitated from the liquid simulant and the off-gas condensate (as applicable).

Aliquots of the final phases post-evaporation were collected and analyzed with ICP-OES, IC, TOC/TC, X-ray Diffraction (XRD), Scanning Electron Microscopy (SEM), and Transmission Electron Microscopy (TEM). The analytical analysis assigned depended on the nature of the final phase (liquid versus precipitate). GEA counting was performed on samples spiked with ^{137}Cs.

3.6 Sample Analysis

For ion exchange testing, cesium load performance was determined from the ^{137}Cs measured in the collected samples relative to the initial ^{137}Cs in each simulant feed. The collected samples were analyzed directly to determine the ^{137}Cs concentration using GEA. Cesium loading breakthrough curves for both the lead and lag columns were generated based on the feed ^{137}Cs concentration (C_0) and the effluent Cs concentration (C) in terms of % C/C_0.

A feed sample for each simulant was collected and analyzed by anion analysis by IC (F^-, Cl^-, NO_2^-, NO_3^-, and PO_4^{3-}), TOC/Total Carbon, and Al, Na, and K analysis by ICP-OES in order to confirm the prepared matrix. Inductively coupled plasma mass spectrometry (ICP-MS) was utilized to analyze ^{133}Cs concentrations.

Analytical services were responsible for the preparation and analysis of appropriate analytical batch and instrument quality control samples and for providing any additional processing to the sub-samples that might be required (e.g., acid digestion, dilutions). All analyses were conducted according to the analytical services standard operating procedures, the QA Plan, and the analytical request.

Simulant samples for the evaporation process spiked with ^{137}Cs were submitted for GEA pre- and post-evaporation process to determine the ^{137}Cs concentration.

Post-evaporate crystalline material generated was analyzed by XRD. The XRD was performed using a Rigaku Ultima IV diffractometer, configured with a 5 degree 2-theta linear position sensitive detector. A sealed tube Cu K-alpha X-ray source operated at 40 kV and 40 mA was used. A Ni-filter reduced the contributions of other X-ray energies. Data was collected with a 0.02-degree step size and a 1 degree/min scan rate. Phase identification was completed with DIFFRAC.EVA software (Bruker version 6.0.0.6) in conjunction with the ICDD PDF-5 database. Phase quantification via Rietveld refinement was performed using the DIFFRAC.TOPAS (Bruker version 6) software package.

Crystalline material was also analyzed using SEM and Polarized Light Microscopy (PLM). All SEM images and PLM data was collected and obtained on a FEI Quanta 250FEG equipped with an Energy Dispersive X-ray Spectroscopy (EDS) system running Genesis software, and a Nikon 400POL with a Nikon digital camera running Elements software.

4.0 Results

This section discusses the Cs exchange behavior during column and batch contact testing with AN-101 and AN-106 representative simulants and the evaporation results with the five simulants developed. Ion exchange process raw data are provided in Appendix A. Batch Contact raw data are provided in Appendix B. Appendix C presents the full post-evaporation material loss analysis, and Appendix D presented the XRD patterns.

4.1 Ion Exchange Column Processing

The Cs load behavior for the 5.5 M Na Al simulant was evaluated at 20 °C. This section discusses the Cs load behavior for the executed test.

4.1.1 Cs Load Results

The 5.5 M Na Al simulant was processed at nominally 1.93 BV/h through the lead and lag columns for 637 BVs. Figure 4.1 shows the Cs breakthrough profiles using a probability log scale plot. The C_0 value for ^{137}Cs was determined to be 1.25E-03 µCi/mL.

The Cs breakthrough from the lead column was observed to start at ~200 BVs and continued to 4% C/C_0 after processing 637 BVs when the last sample was collected from the lead column. There was no discernable breakthrough on the lag column. Also shown on the graph is a 50% C/C_0 indication line (shown in red), and the WAC limit, set at 0.1% C/C_0 (dashed black line).

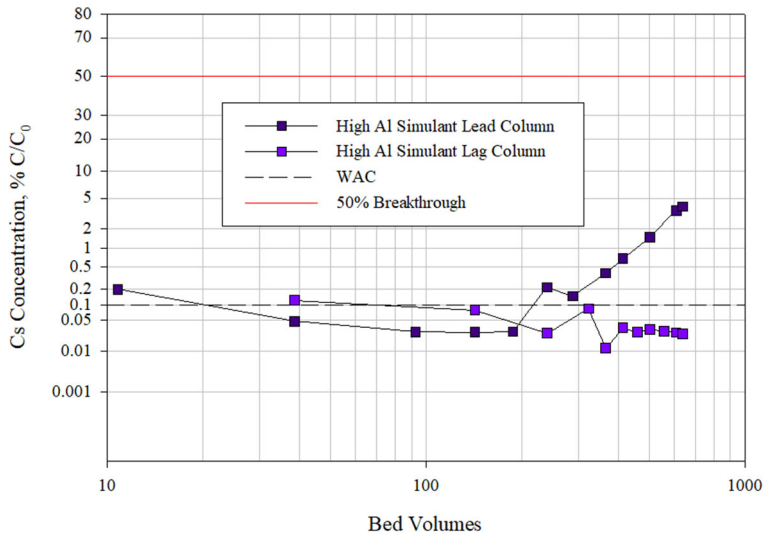

Figure 4.1. Lead and Lag Column Cs Load Profiles of 5.5 M Na Al Simulant at 1.9 BV/h

The Cs breakthrough curve for the lead column was modeled by the error function (erf) (Hougen and Marshall 1947; Klinkenberg 1948), as shown in Eq. (4.1):

$$\frac{C}{C_0} = \frac{1}{2}\left(1 + \mathrm{erf}\left(\sqrt{k_1 t} - \sqrt{k_2 z}\right)\right) \quad (4.1)$$

where:

k_1 and k_2 = parameters dependent on column conditions and ion exchange media performance
t = time (or BVs processed)
z = column length

Using this model, a fit was generated to the lead column experimental data in Figure 4.2. The k_1 and k_2 values for the lead column were found to be 97.7 and 14.4, respectively.

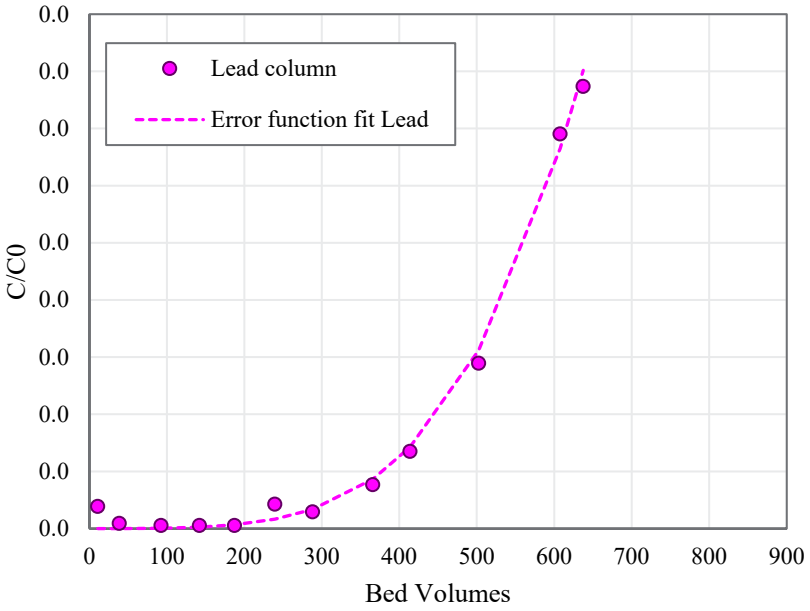

Figure 4.2. AN-107 Lead and Lag Column Cs Breakthrough with Error Function Fit

The 50% Cs breakthrough for the lead column was estimated from the error function fit at 1405 BVs. The theoretical 50% Cs breakthrough on the ion exchange column (λ) can be predicted from the product of the K_d value and the ion exchanger bed density (ρ_b) according to Eq. (4.2) (Bray et al. 1993). The CST bed density is the dry CST mass divided by the volume in the column:

$$K_d \times \rho_b = \lambda \quad (4.2)$$

The current TSCR Waste Acceptance Criteria (WAC) of 3.18E-5 Ci ^{137}Cs/mole of Na limit Cs breakthrough was interpolated for the lead column by curve-fitting the BVs processed as a function of the log % C/C_0 values (see Figure 4.3). The curve was fitted to a second-order polynomial function ($R^2 \geq 0.99$) and the WAC limit breakthrough was then calculated, resulting in a value of 257 BVs for the lead column. Due to no significant breakthrough on the lag column, a WAC value was not determined.

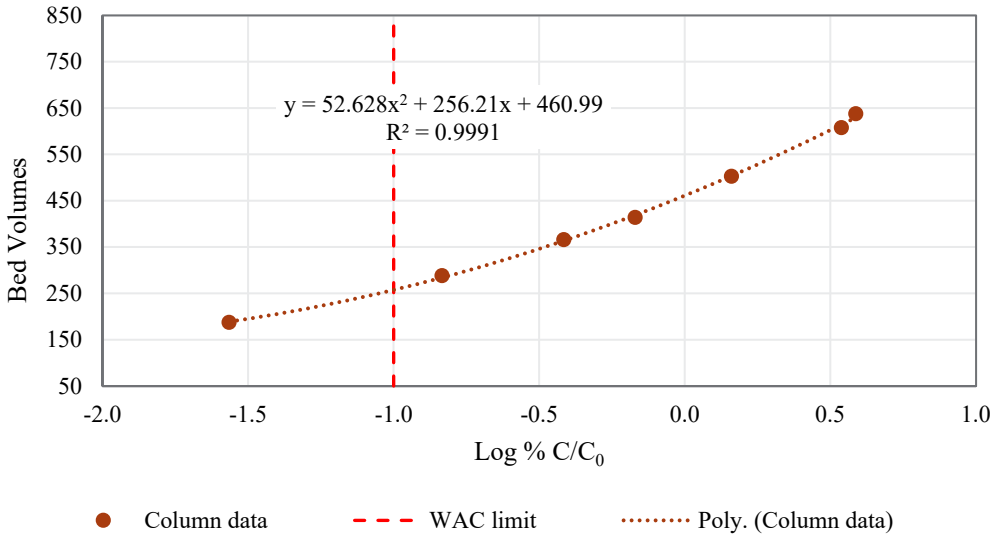

Figure 4.3. Curve Fits to Interpolate WAC Limit Breakthroughs from 5.5 M Na Al Simulant Lead Column

4.1.2 Cesium Activity Balance

The Cs fractionations to the effluent and the columns were determined based on the input ^{137}Cs and the measured ^{137}Cs in the various effluent streams. The quantities of Cs loaded onto the lead and lag columns were determined by subtracting the Cs recovered in the samples and effluents from the Cs fed to each column. Table 4.1 summarizes the ^{137}Cs fractions found in the various effluents as well as the calculated ^{137}Cs column loadings. As to be expected based on the breakthrough curves, nearly all the total Cs loaded onto the lead column with only 0.8% loading onto the lag column. Sample and effluent collection amounted to only ~0.03% of the input Cs.

Table 4.1. ^{137}Cs Activity Balance for 5.5 M Na Al Simulant

Input		
	µCi	%
Feed Sample	5.17E+00	100.0
Output		
Effluent	1.12E-03	0.02
Load samples	4.24E-04	0.01
Feed displacement, water rinse and flush	1.95E-04	0.00
Total ^{137}Cs recovered in effluents	1.74E-03	0.03
Total ^{137}Cs column loading		
Lead column Cs loading	5.17E+00	100.0
Lag column Cs loading	4.01E-02	0.8
Activity balance	5.21E+00	1.0

The total Cs loaded per g CST was calculated from the total Cs loaded onto the lead column and the dry CST mass loaded into the lead column according to Eq.(4.3):

$$\frac{A_{Cs} \times CF}{M} = C \quad (4.3)$$

where

A_{Cs} = activity of ^{137}Cs, µCi on the lead column
CF = conversion factor, mg Cs/µCi ^{137}Cs
M = mass of dry CST (6.0 g)
C = capacity, mg Cs/g CST

A total of 6.21 mg Cs/g CST (0.0467 mmoles Cs/g CST) was loaded onto the lead column. Since only a fraction of the column's capacity was actually loaded during testing, the 50% breakthrough value (calculated per Eq. (4.2)) can be used to determine the full load capacity. This value was calculated to be 13.09 mg Cs/g CST (0.0985 mmoles Cs/g CST). The documented safety analysis (DSA) currently employed at TSCR limits a single column curie loading to 141,600 Ci, which equates to 0.10 mmole Cs/g CST. The total load capacity determined for the column testing represented 98.5% of this limit and indicates that if processing occurs ≥20 °C, the curie limit on the lead column will not exceed this threshold prior to WAC breakthrough on subsequent columns; however, drops in temperature will increase loading and will likely exceed this current DSA loading restriction.

4.1.3 High Al Simulant Performance Comparison

Figure 4.4 provides the 5.5 M Na Al simulant column load profiles alongside previously processed AP-107 tank waste supernate (Fiskum et al. 2019b) for a direct loading comparison. Testing parameters for the simulant and tank waste matrices are shown in Table 4.2. The Cs exchange associated with the high Al simulant resulted in a later Cs breakthrough for the lead column to reach the WAC by nominally 25%. As breakthrough progresses out towards the 50% breakthrough point, a larger deviation in BVs processed becomes apparent. As determined above, capacity for the 5.5 M Na Al simulant was calculated to be 13.09 mg Cs/g CST, AP-107 testing resulted in a capacity value of 8.24 mg Cs/g CST. With these values, the simulant represents 159% of the AP-107 CST capacity. Given the largest deviations in matrix come from the K, it is likely due to the decrease in K concentration in the simulant by nearly 97%, which increases the capacity for Cs onto the CST. Temperature deviations between the two tests likely also play a role, with a decreased temperature for the simulant run by 7 °C increasing the capacity for Cs onto the CST. Additionally, the kinetics for the simulant test appear slightly slower than AP-107, based on a lesser slope in the load curve for the lead column. This may be due to differences in waste chemistry attributed to the higher aluminum concentration in the simulant.

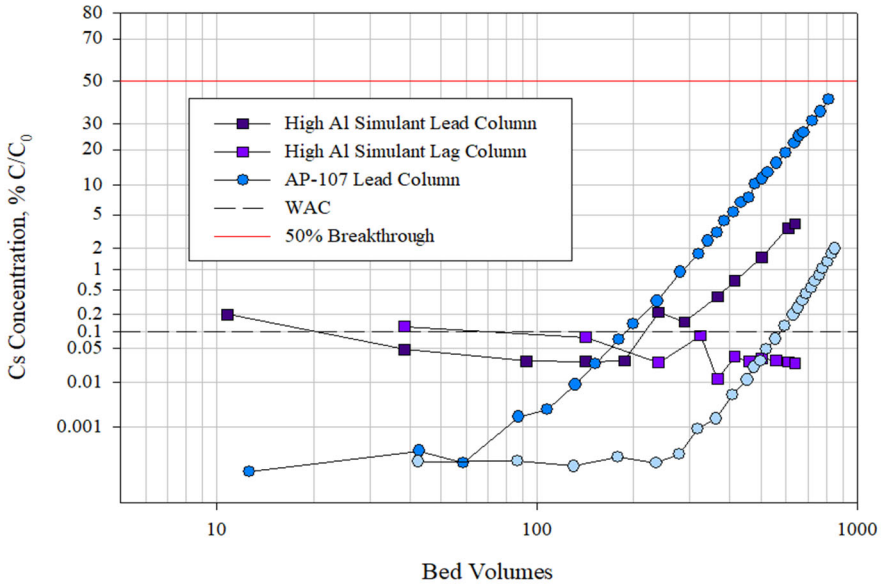

Figure 4.4. Comparative Cs Breakthrough Performance for 5.5 M Na Al Simulant and AP-107, Probability-Log Plot

Table 4.2 High Al Simulant and AP-107 Tank Waste Supernate Testing Parameters

Testing Condition	5.5 M Na Al Simulant (Current)	AP-107 (FY21)
Configuration	Lead-Lag	Lead-Lag-Polish
Flowrate, BV/h	1.93	1.91
Process Temp. °C	20.2	~27.0
Density, g/mL	1.25	1.26
WAC limit, $\%C/C_0$	0.10	0.12
Lead column BVs to WAC	257	200
Cs, M	7.01E-05	6.84E-05
Na, M	5.35	5.97
NO_3	1.63	1.71
NO_2	1.01	1.14
PO_4	0.016	0.017
CO_3	0.513	0.645
K, M	0.04	0.12
Al, M	0.511	0.371

4.2 Batch Contacts

This section provides the K_d and isotherm curves for each of the PO_4 and F simulants at variable Na, PO_4, and F concentrations as well as a comparison of the data with AP-107 sodium-dependent isotherm results. Input data supporting the various isotherms and figures are provided in Appendix B.

4.2.1 K_d and Isotherm Results for Avg PO_4/F Simulant

Figure 4.5 shows the K_d dependence on Cs concentration for the Avg PO_4/F Simulant at target Na concentrations of 0.5 M, 1.0 M, 2.0 M, 3.0 M, and 3.5 M Na. As to be expected, the K_d increased with decreasing Na concentration. There is negligible change in the K_d for the three lowest Cs concentrations (3.3E-5 M, 1.3E-4 M, 7.8E-4 M) measured. This behavior has also been observed for tank waste supernate matrices (Westesen et al. 2024) and suggests the K_d is unimpacted with small changes in Cs concentrations of $<10^{-3}$ M Cs.

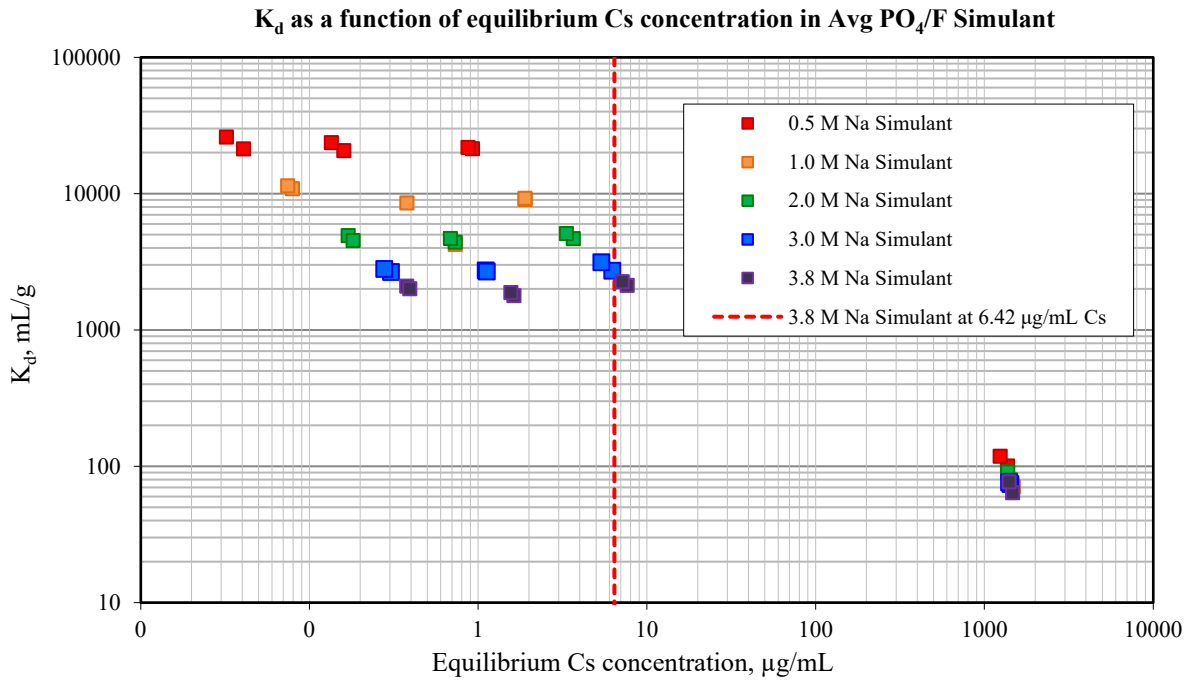

Figure 4.5. Cs K_d vs. Cs Concentration, Avg PO_4/F Simulant, Five Na Concentrations

Figure 4.6 shows the corresponding isotherms and Q (mmoles Cs/g dry CST) values vs. Cs molarity at all five Na concentrations. It is important to note that the α_i, or total capacity in the matrix, was set to 0.68 mmoles Cs/g CST for this evolution of testing. Also provided are the curve fits to the Freundlich/Langmuir hybrid equilibrium model as given in Eq. (4.4) (Hamm et al. 2002).

$$Q = \frac{\alpha_I \times [Cs]}{(\beta + [Cs])} \qquad (4.4)$$

where

[Cs] = equilibrium Cs concentration, mmoles/mL or M
Q = equilibrium Cs loading on the CST, mmole Cs per g CST
α_i = isotherm parameter constant (mmoles/g), equivalent to total capacity in the matrix
β = isotherm parameter constant (mmoles/mL or M), selectivity coefficient, dependent on matrix and temperature; the larger the value, the less selective the CST is for Cs (Hamm et al. 2002)

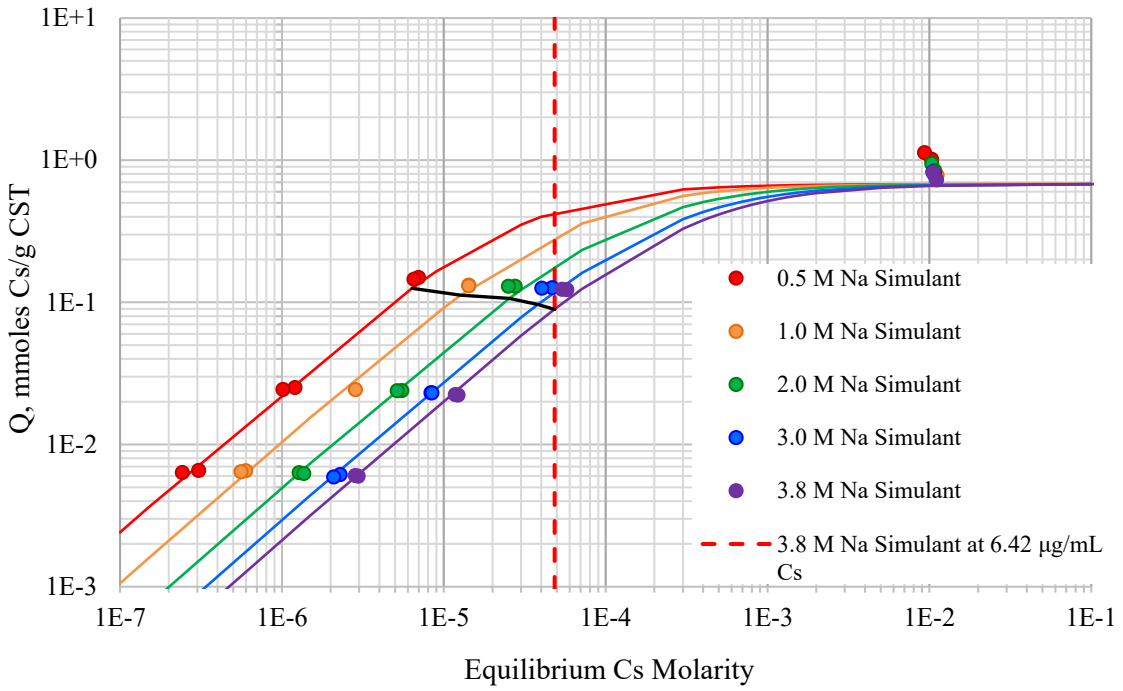

Figure 4.6. Q vs. Cs Equilibrium Concentration, Avg PO_4/F Simulant with Freundlich/Langmuir Hybrid Equilibrium Fits, Five Na Concentrations. The dashed red line represents the estimated Cs concentration (4.83E-5 M) in AN-101 and AN-106 supernate adjusted to 3.8 M Na.

The initial feed concentration of 7.8E-04 M Cs most closely resembles the Cs feed concentration estimated from AN-101 and AN-106 tank waste supernate at 3.8 M Na, which is represented by the dashed line in Figure 4.6. In the current flowsheet planning for DFHLW, the sludge is diluted down to achieve a nominal 1.3 g/mL specific gravity (SG) (~3.8 M Na). Looking at the results from the batch contacts with the Avg PO_4/F simulant, the Cs loading (Q, mmoles/g) at 3.8 M Na is 0.089 mmoles Cs/g CST vs. 0.43 mmoles Cs/g CST at 0.5 M Na. This equates to a 73% difference in Cs loading between 3.8 and 0.5 M Na. However, diluting the 3.8 M Na down to 0.5 M Na also results in a volume increase of 87%. A dilution line with loading for each of the Na concentration tested is shown in Figure 4.7. These results are also compared to AP-107 supernate dilution testing from 8.0 M Na down to 3.5 M Na in Figure 4.8 and show good agreement in the overall Cs uptake behavior with variable Na concentration. These results provide valuable information from a processing standpoint on what concentration of Na would optimize Cs removal, maximize dissolution and HLW vitrification efficiency, as well as minimize secondary waste or additional process steps.

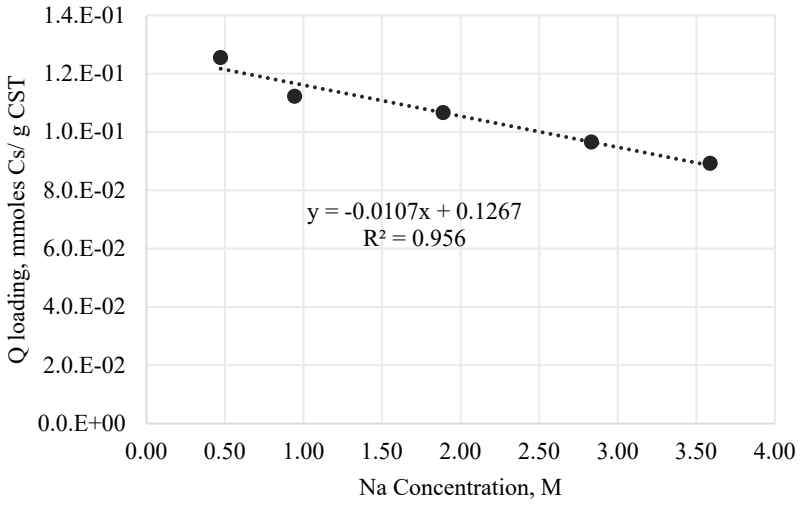

Figure 4.7. Q vs. Na Concentration for Avg PO4/F Simulant

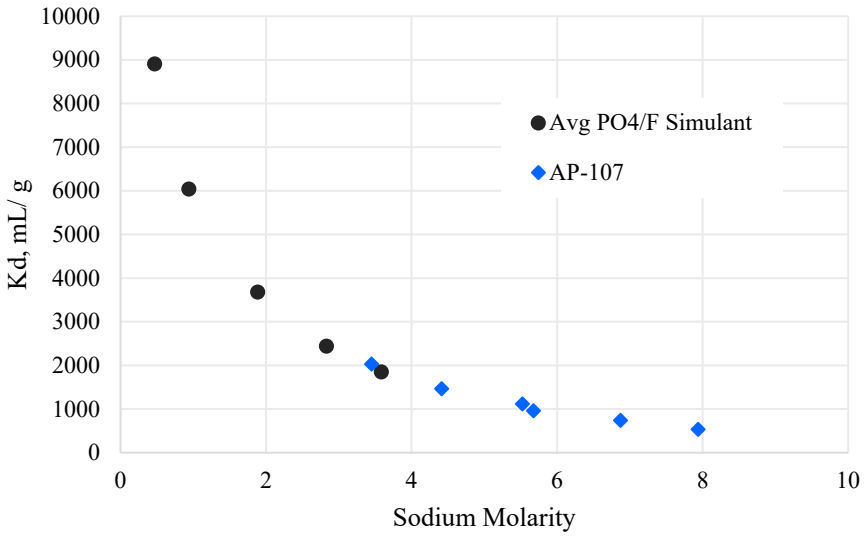

Figure 4.8. K_d vs. Na Concentration for PO4/F Simulant and AP-107

4.2.2 K_d and Isotherm Results for Low PO_4/High F, High PO_4/Low F Simulant, and 1.9 M Na Washed PO4/F Simulant

Figure 4.9 shows the K_d dependence on Cs concentration for the Low PO_4/High F, High PO_4/Low F Simulant, and 1.9 M Na Washed PO_4/F Simulant. Similarly to what was found for the variable Na contact, the K_d for the 1.9 M Na simulant was higher overall than both the 3.8 M Na high PO_4/low F and low PO_4/high F simulants. Again, consistent with the variable Na batch contacts, there appears a negligible change in the K_d for the three lowest Cs concentrations (3.3E-5 M, 1.3E-4 M, 7.8E-4 M) measured.

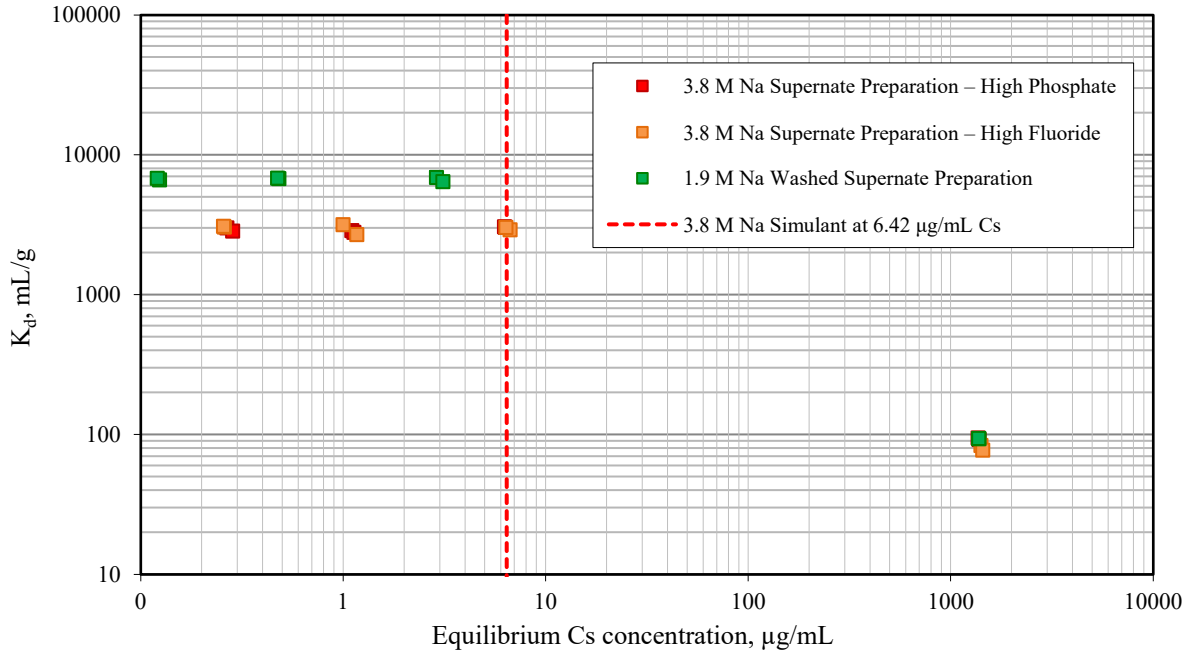

Figure 4.9. Cs K_d vs. Cs Concentration, Avg PO_4/F Simulant, Five Na Concentrations

Figure 4.10 shows the corresponding isotherms and Q (mmoles Cs/g dry CST) values vs. Cs molarity for each matrix. Also included on this figure is the 3.8 and 2.0 M Na Avg simulant results from Figure 4.6.

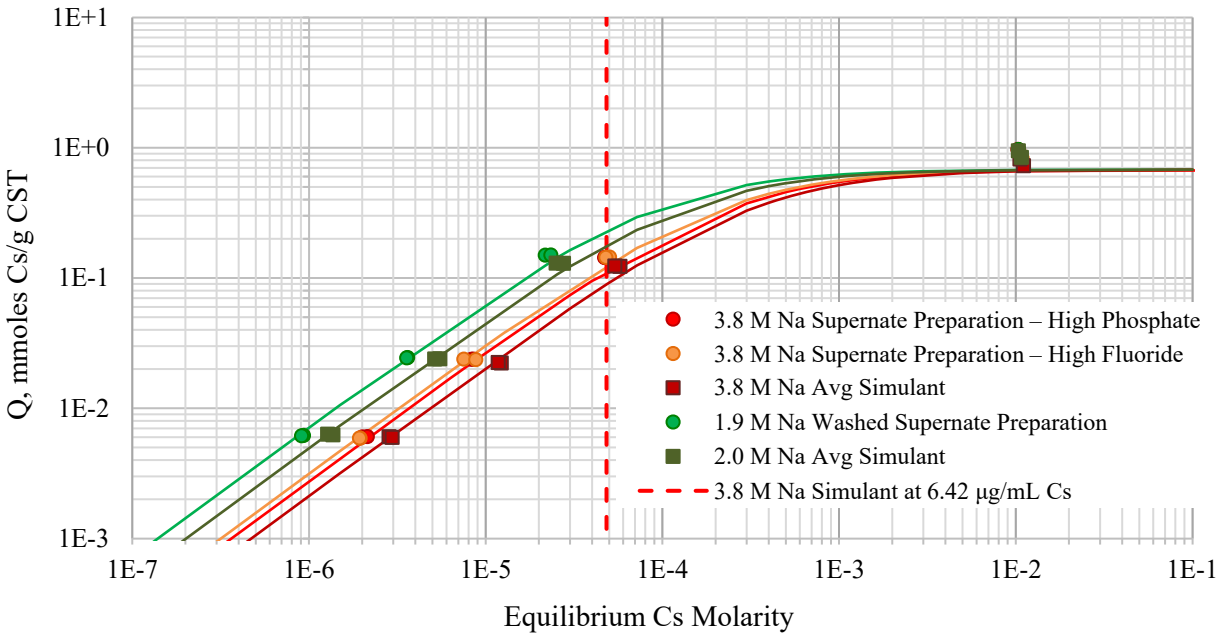

Figure 4.10. Q vs. Cs Equilibrium Concentration, High PO_4/Low F, Low PO_4/High F, 1.9 M Na Avg Washed Simulant with Freundlich/Langmuir Hybrid Equilibrium Fits.

Negligible difference was seen between the Low PO_4/High F and High PO_4/Low F simulants indicating no specific anion impact on the Cs removal. The 1.9 M Na washed supernate contained higher amounts of PO_4 and F compared to the 2.0 M Avg simulant and displayed the best overall Cs uptake of the batch and may be attributed to the slightly lower Na concentration in the matrix. Figure 4.11 displays the same dilution curve as Figure 4.8 but with the inclusion of the additional PO_4 and F batch contact data. From this graph we can infer the slight differences in loading are likely due to variations in Na concentration vs anion concentration in the feeds.

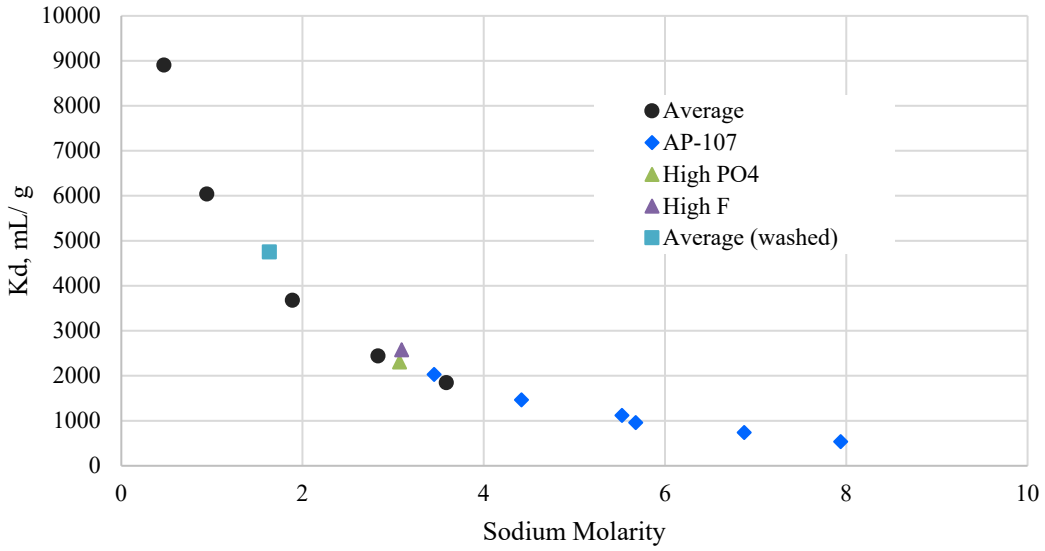

Figure 4.11. K_d vs. Na Concentration for All PO_4/F Simulants with AP-107

4.3 Evaporation Results

4.3.1 Post-Evaporation Collection

The initial starting mass of the simulant, as well as the gross mass of resulting phases collected post filtration are given in Table 4.3. The mass loss in the system was also estimated and presented in Table 4.3. Following evaporation, the solid crystal phase was collected. Visually, the crystalline material was a white salt compound. No distinct features were noted on the crystals, as seen in Figure 4.12. The quantity of crystal material slightly varied as the higher PO_4^{3-} simulant resulted in the largest amount of crystal material (50.2 g). The low PO_4^{3-} simulant resulted in very minimal generated crystal material (0.040 g), which also took an extended period of time to generate. The runs with the average simulant ranged from 21.8 g to 34.7 g of solid material generated.

Table 4.3 Final Phase Collection Post-Evaporation

Phase / Simulant Matrix	Starting Mass	Post-Evaporate Concentrate	Off-Gas Condensate	Crystalline Phase	Mass Loss
	Mass, g				
Average PO_4^{3-}/F^- Simulant	2354.0	1602.2	624.0	21.8	106.0
High PO_4^{3-}/Low F^- Simulant	2354.2	1546.9	645.4	50.2	111.7
Low PO_4^{3-}/High F^- Simulant	2344.0	1651.5	622.2	0.040	70.3
Average PO_4^{3-}/F^- with $CsNO_3$ Simulant	2355.0	1604.6	637.5	34.7	78.2
Average PO_4^{3-}/F^- with $CsNO_3$ and ^{137}Cs Simulant	2355.7	1591.5	399.5	24.3	340.4

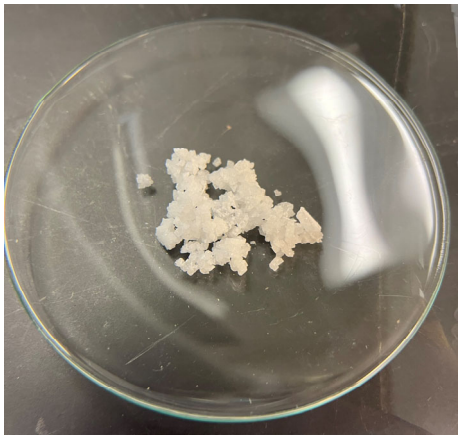

Figure 4.12 White Crystal Material Collected Post-Evaporation.

4.3.2 Liquid Analysis

The final evaporator concentrate measured between 4.78 M Na and 5.39 M Na with a pH >13. The evaporated simulant concentrate had a calculated density of nominally 1.26 g/mL for the three matrices studied with the absence of Cs. The off-gas contained few detectable components and had a pH of 4-5 with a density of ~1.0 g/mL. Full compositional analysis of the two resulting liquid phases for each simulant matrix are presented in Table 4.4, where PE is post-evaporate concentrate, and Conds. is for the off-gas condensate.

Table 4.4 Post-Evaporate Analytical Analysis of Liquid Phases

Simulant	Average PO_4^{3-}/F^- Simulant		High PO_4^{3-}/Low F^- Simulant		Low PO_4^{3-}/High F^- Simulant		Average PO_4^{3-}/F^- with $CsNO_3$ Simulant		Average PO_4^{3-}/F^- with $CsNO_3$ and ^{137}Cs Simulant	
Calculated Concentration, mol/L										
Ion	PE Sim.	Off-Gas Conds.	PE Sim.	Off-Gas Conds.	PE Sim.	Off-Gas Conds.	PE Sim.	Off-Gas Conds.	PE Sim.	Off-Gas Conds.
Al^+	0.11	ND	0.02	ND	0.11	ND	0.13	ND	0.12	ND
F^-	0.05	1.5E-04	0.01	ND	0.12	ND	0.05	ND	0.05	ND
Cl^-	0.05	3.2E-05	0.05	5.1E-05	0.06	3.5E-05	0.05	4.6E-05	0.04	ND
K^+	0.05	ND	0.05	ND	0.06	ND	0.05	ND	0.05	ND
NO_2^-	1.53	ND	1.48	ND	1.35	ND	1.57	ND	1.65	ND
NO_3^-	1.03	ND	0.44	ND	1.30	ND	1.07	3.0E-05	1.07	ND
PO_4^{3-}	0.03	3.5E-04	0.12	ND	0.02	ND	0.03	ND	0.02	ND
CO_3^{2-}	0.16	ND	0.23	ND	0.16	ND	0.16	ND	0.18	ND
Na^+	4.78	ND	4.96	1.4E-03	5.18	1.2E-03	5.18	0.03	5.39	ND
Cs^+	N/A	N/A	N/A	N/A	N/A	N/A	5.31E-04§	8.13E-08§	7.1E-10‡	ND

Analytes not included in the simulant matrix are marked as N/A.
§Cs-133 mass calculated through ICP-MS.
‡Cs-137 mass calculated through GEA.

The mass balance of the individual ion masses was tracked between the initial simulant, the post-evaporation concentrate and post-evaporation off-gas condensate. The % loss of the individual ions are shown in Table C-1 through Table C-5 for the different sample matrices and simulant compositions.

Focus on the mass loss or gains in the phosphate and fluoride ions are of most interest with respect to generation of natrophosphate, as presented in Table 4.5. Any material lost is presumed to have been incorporated with the crystal material generated, as the content of the off-gas condensate did not contain an appreciable amount of any components.

Natrophosphate is a congruent double salt, meaning the Na:F:PO_4 mol ratios in the liquid phase in equilibrium with the pure salt are the same as in the solid phase. It is less soluble than the single salts NaF or Na_3PO_4. Fluoride has a large impact on the properties of a slurry containing phosphate. With fluoride present the double salt forms, and slurry viscosity is reduced due to the crystal habit which is more compact; fluoride absence results is phosphate solids that have a needle appearance and a high viscosity (Herting et al. 2015).

Mole content analysis of the material lost by ion illustrates the potential for new species generated from the lost material. The starting average simulants contained equimolar amounts of F^- and PO_4^{3-}. Post-evaporation, the F^-: PO_4^{3-} mol ratio was ~1:2 for the three average simulants, 1:9 for the high PO_4^{3-} run, and 2:1 for the low PO_4^{3-} run. These results suggest that other PO_4^{3-} phases may precipitate along with the naturophosphate; or that polymorphs are generated.

Table 4.5 Percent Loss of F^- and PO_4^{3-} Species in the Post-Evaporate Simulant Remaining

	Percent Loss Relative to Starting Simulant, %		Mol Difference Relative to Starting Simulant, mol	
Simulant	F^-	PO_4^{3-}	F^-	PO_4^{3-}
Average PO_4^{3-}/F^- Simulant	33.9%	59.2%	0.03	0.06
High PO_4^{3-}/Low F^- Simulant	24.1%	37.3%	0.01	0.09
Low PO_4^{3-}/High F^- Simulant	8.9%	-37.3%	0.02	0.01
Average PO_4^{3-}/F^- with $CsNO_3$ Simulant	33.5%	62.5%	0.04	0.07
Average PO_4^{3-}/F^- with $CsNO_3$ and ^{137}Cs Simulant	36.7%	71.6%	0.04	0.08

The mass of the Cs material was tracked through the evaporation process to understand how it is partitioning in the evaporation process, further shown in Table C-4. Minor amounts were measured in the off-gas condensate collected and the crystalline material through ICP-MS analysis of the final ^{133}Cs materials and GEA of the ^{137}Cs materials. The measured ^{137}Cs on the solid sample was likely due to residual liquid on the material at collection. Further to this, no Cs was detected in the microscopy analysis.

The Cs is largely remaining in the post-evaporate simulant solution. The post-evaporate simulant noted a 7.7% loss of ^{133}Cs in the non-radiological Cs experiment from the starting simulant. The process run with the ^{137}Cs spike exhibited a 10.7% loss of Cs material from the starting simulant to the post-evaporate simulant remaining. Both results illustrate that the Cs largely remains within the liquid post-evaporate phase.

4.3.3 X-Ray Diffraction of Crystal Material

XRD patterns were collected for the crystalline material generated in each evaporation run, with the exception of the low PO_4^{3-}/high F^- simulant as there was not enough crystal material generated.

The XRD patterns quantified the composition of the crystalline material generated and provided a better understanding of the compound. Table 4.6 presents the quantification of the matrices by wt%. All resulting diffraction patterns are located in Appendix D, Figure D-1 through Figure D-4. The average PO_4^{3-}/F^- simulant was quantified as containing 91 wt% $Na_7FPO_4 \cdot 19H_2O$, with 6 wt% $Na_2CO_3 \cdot H_2O$, and 3 wt% $NaNO_2$, shown in Figure D-1. The observed diffraction pattern in the average simulant containing only $CsNO_3$, was similar with 92 wt% $Na_7FPO_4 \cdot 19H_2O$, 4 wt% $Na_2CO_3 \cdot H_2O$, and 4 wt% $NaNO_2$ (Figure D-3). Finally, diffraction patterns collected for the average PO_4^{3-}/F^- simulant with $CsNO_3$ and ^{137}Cs spike were collected, Figure D-4. Composition of this sample was consistently quantified in relation to the other average matrices and was quantified as having 92 wt% $Na_7FPO_4 \cdot 19H_2O$, 4 wt% $Na_2CO_3 \cdot H_2O$, and 2 wt% $NaNO_2$, and additionally 2 wt% Na_2HPO_4, which was not observed in other sample pattern collections.

The high PO_4^{3-}/low F^- simulant provided a very busy diffraction pattern, as observed in Figure D-2. While the identity of the crystal material was mostly natrophosphate, like the prior average simulants collected, there was a contribution from another product that could not be identified fully. The main components identified based on the simulant composition are noted in Table 4.6. Outside of the minor amount of dihydrogen phosphate there was no measurable amount of other phosphate phases which would account for the variation in molar ratio.

Table 4.6 XRD Component Quantification by wt%

	Component wt%			
Simulant	$Na_7FPO_4 \cdot 19H2O$	$Na_2CO_3 \cdot H2O$	$NaNO_2$	Other
Average PO_4^{3-}/F^- Simulant	91	6	3	N/A
High PO_4^{3-}/Low F^- Simulant	86	9	5	N/A
Low PO_4^{3-}/High F^- Simulant	N/A	N/A	N/A	N/A
Average PO_4^{3-}/F^- with $CsNO_3$ Simulant	92	4	4	N/A
Average PO_4^{3-}/F^- with $CsNO_3$ and ^{137}Cs Simulant	92	4	2	2 wt% Na_2HPO_4

4.3.3.1 Microscopy Analysis of Crystal Material

PLM images were collected for the crystal material generated from all five matrices. Images were taken with crossed polars and a ¼ waveplate. Images collected, Figure 4.13, differed depending on the starting simulant. Birefringent particles, i.e., translucent clear particles, were common to all resulting images.

A. Average PO_4^{3-}/F^- Simulant: crystal material showed many low birefringent particles at 20× magnification.

B. High PO_4^{3-}/Low F^- Simulant: crystal material was dominated by high birefringent needle like crystals at 20×. Crystals were mounted in collodion, which has a refractive index of 1.5, and would be similar to the mounting used in PLM studies by Bolling et al. (Bolling et al. 2020).

C. Low PO_4^{3-}/High F^- Simulant: images showed fibrous structures as well as isolated particles at 20×.

D. Average PO_4^{3-}/F^- Simulant with $CsNO_3$: crystal material images showed a sufficient number of high birefringent particles at 20×, making interpretation difficult. The sample had a more complex series of phases compared to the other samples examined.

E. Average PO_4^{3-}/F^- Simulant with $CsNO_3$ and ^{137}Cs: low birefringent particles in the images are suggestive of natrophosphate.

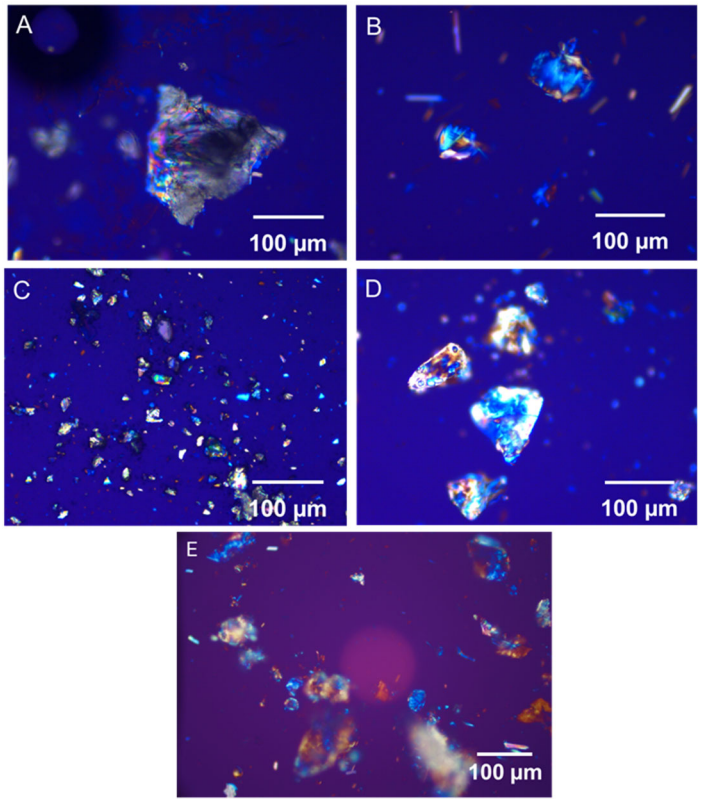

Figure 4.13 Polarized Light Microscopy of Natrophospate Crystal Material. (A) Average PO_4^{3-}/F^- Simulant, (B) High PO_4^{3-}/Low F^- Simulant, (C) Low PO_4^{3-}/High F^- Simulant, (D) Average PO_4^{3-}/F^- with $CsNO_3$ Simulant, and (E) Average PO_4^{3-}/F^- with $CsNO_3$ and ^{137}Cs Simulant.

Natrophosphate is easily distinguishable using SEM analyses due to the larger size and the shape of the crystals formed. Fluoride has a large impact on the properties of a slurry containing phosphate. With fluoride present, the double salt forms, and slurry viscosity is reduced due to the crystal habit which is more compact; fluoride absence results is phosphate solids that have a needle appearance and a high viscosity (Herting et al. 2015). Scanning electron microscopy of the materials produced illustrated a variety of material shapes and structures, as shown in Figure 4.14.

For the Average PO_4^3/F^- simulant crystal material (A and B in Figure 4.14), various morphologies were illustrated. Plate-like structures were identified in regions as well as interspersed rod structures. Decreasing magnification illustrated thick, stacked plates with fibrous looking material.

The High PO_4^{3-}/Low F^- simulant (C and D in Figure 4.14) occurred in large acicular rod-like particles, which is consistent with the PLM observations. Decreasing magnification showcases plates, similar to that observed in the Average PO_4^3/F^-crystal results.

The Low PO_4^{3-}/High F^- simulant exhibited structures that differed highly from all other simulant matrices (E and F in Figure 4.14). The material looked to occur in large ball structures as high magnifications and showed a fibrous appearance. Smaller high contrast particles were observed nested within the fiber structures. At decreasing magnifications, acicular crystal forms were observed.

The Average PO_4^{3-}/F^- with $CsNO_3$ occurred as thick particles with cracks running throughout, possibly indicating dehydration from the vacuum system (G and H, Figure 4.14). Like that observed in the Average PO_4^{3}/F^- and the High PO_4^{3-}/Low F^- simulant crystal results, bundles of plates could be observed at decreasing magnifications.

Images collected from the Average PO_4^{3}/F^- with $CsNO_3$ with ^{137}Cs exhibited images and a structure that differed again from the other simulant matrices. However, the structures observed are consistent with observed natrophosphate within tank waste and simulant studies (Herting et al. 2015).

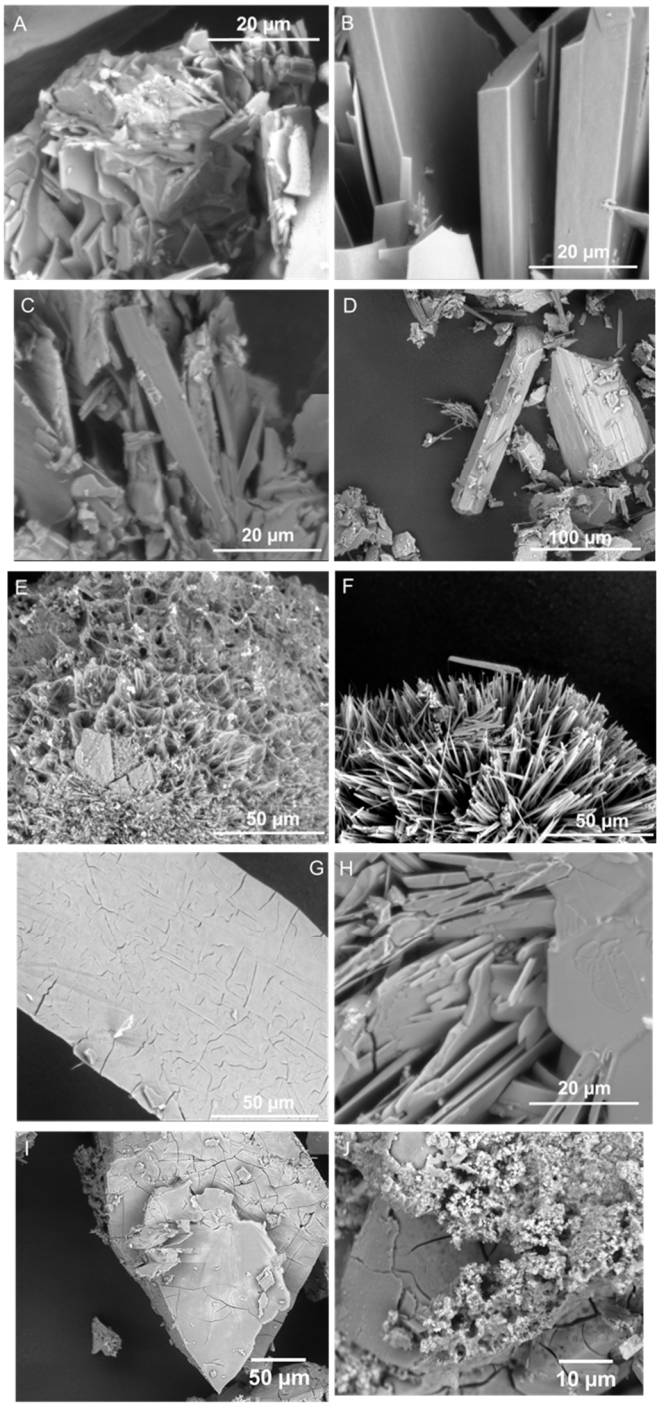

Figure 4.14 Scanning Electron Microscopy of the Crystal Material. A and B: Average PO_4^{3-}/F^- Simulant; C and D, High PO_4^{3-}/Low F^- Simulant; E and F, Low PO_4^{3-}/High F^- Simulant; G and H, Average PO_4^{3-}/F^- with $CsNO_3$ Simulant; I and J, Average PO_4^{3-}/F^- with $CsNO_3$ and ^{137}Cs Simulant. Images collected at 10 keV, Back Scattered Electron (BSE) Imaging, low vacuum, working distance (WD) = 10 mm, spot = 5.5 at 5000×, 2000×, and 1000×.

5.0 Conclusions

Cesium ion exchange column, batch contact, and evaporator testing was conducted with various simulant matrices to determine an effective disposition of sludge washing leachate. Overall, sludge leachate solutions retrieved at or near their solubility limits for either phosphate or fluoride (or both) can be effectively processed through CST ion exchange columns in order to dispose of the supernate through WTP LAW. Solutions may be evaporated up to 5.5 M Na to minimize the waste volume sent to LAW and a crystallized natrophosphate salt can be removed prior to Cs removal and vitrification operations. Conclusions of the results are provided below.

5.1 High Al Simulant Column Testing

A 5.5 M Na Aluminum simulant prepared to represent a gibbsite leachate solution was processed through two columns sequentially positioned in a lead-lag format. Each column was filled with 6.0 mL of CST ion exchanger. A total of 3.7 L of simulant was processed through the Cs ion exchange system at 1.93 BV/h and 20 °C. Effluent samples were collected periodically from each column during the load process and measured for ^{137}Cs to establish the Cs load curves. The flowrate was increased to 3.0 BV/h to process 12.0 BVs each of 0.1 M NaOH feed displacement solution and water rinse. The following conclusions were drawn from the results of this work:

1. Testing showed that at 20 °C, 1405 BVs of 5.5 M Na Al simulant, processed at 1.93 BV/h, was calculated to be treated before reaching 50% Cs breakthrough on the lead column. No significant breakthrough occurred on the lag column after processing 637 BVs of simulant.
2. The WTP LAW WAC limit for the 5.5 M Na Al simulant lead column was reached nominally 60 BVs later than respective lead column breakthrough with AP-107 tank waste at 27 °C (Fiskum et al. 2019b). Variations in feed matrices (namely K concentration) as well as temperature differences are likely responsible for the deviation in BVs processed to reach the WAC.
3. The total theoretical Cs loading onto the lead column (13.09 mg Cs/g CST) was notably higher than that seen in previous AP-107 testing (8.24 mg Cs/g CST) at the same processing flowrate and is likely due to increased Cs loading capacity due to the notably lower K concentration and lower processing temperature.

5.2 PO_4/F Simulant Batch Contact Testing

Cs isotherms were developed for four distinct PO_4 and F simulants as well as five different Na concentrations. Batch contacts were executed at 20 °C with Cs concentrations of 3.3E-5 M, 1.3E-4 M, 7.8E-4 M, and 1.5E-2 M Cs. Batch contacts were conducted in duplicate with 0.075 g dry CST (IONSIV R9140-B, lot 2002009604) per 15 mL of solution and agitated in a temperature-controlled box for ~140 h. The isotherm data were fit to the Freundlich/Langmuir hybrid equilibrium model and the linear Freundlich model to calculate K_d and Q values at approximate AN-101 and AN-106 supernate feed conditions of 4.83E-5 M Cs at 3.8 M Na. Results of the variable Na molarity batch contact testing were compared to AP-107 variable Na molarity studies. The following conclusions were made from this testing:

1. The Freundlich/Langmuir hybrid model accurately predicts the loading for all Cs concentrations chosen to bound the AN-101 and AN-107 predicted feed conditions. To

further explore fidelity of the fit, the linear Freundlich isotherm was also determined to predict loading with $R^2 > 0.99$ for the four Cs concentrations in all matrices.

2. Diluting the 3.8 M Na Avg PO4/F simulant down from 3.8 M Na to 0.5 M Na resulted in a linear decrease in Q. These results indicate little tradeoff in terms of additional Cs removal at a lower Na concentration, however, it also showed additional PO_4 and F in solution at the lower Na concentrations do not hinder Cs uptake.
3. Negligible difference was seen between the Low PO_4/High F and High PO_4/Low F simulants indicating no specific anion impact on the Cs removal. The 1.9 M Na washed supernate contained higher amounts of PO_4 and F compared to the 2.0 M Avg simulant and displayed the best overall Cs uptake of the batch and may be attributed to the slightly lower Na concentration in the matrix.
4. The variable Na molarity batch contacts were compared with those of AP-107 and found consistent agreement in the overall Cs uptake behavior with variable Na concentration under the range of conditions tested.

5.3 Evaporator Testing

Five simulants were prepared for evaporation tests of varying PO_4^{3-} and F^- concentrations. Two of the five runs also contained Cs (^{133}Cs in one, and ^{133}Cs and ^{137}Cs in the second). Evaporation was completed with each simulant under vacuum to represent prototypic operations. Using an evaporator vessel, the solutions were evaporated until nominally ~1.36 L remained in the evaporation feed vessel. Solutions evaporated at approximately 80 °C under 19 in Hg (9.33 psi). The resulting post-evaporate simulant, off gas condensate, and resulting crystalline material was analyzed. These results were analyzed to understand the Cs partitioning in the final materials, and to better interpret the impact of PO_4^{3-} and F^- concentration on the process. Results of the testing showed:

1. The PO_4^{3-} to F^- ratio impacts the degree of precipitation of natrophosphate as expected. Higher phosphate concentrations result in a greater amount of crystal material. Crystal material was generated faster in those samples with average or higher PO_4^{3-} concentrations.

2. Mol content analysis of the material shows the potential for species other than natrophosphate to also be generated. The precipitation process had a molar imbalance. The starting average simulants contained equimolar amounts of F^- and PO_4^{3-}. Post-evaporation, the F^-: PO_4^{3-} mol ratio was ~1:2 for the three average simulants, 1:9 for the high PO_4^{3-} run, and 2:1 for the low PO_4^{3-} run. These results suggest that other PO_4^{3-} phases may precipitate along with the natrophosphate; or that polymorphs are generated.

3. The Cs content tracked between samples shows that the majority of the Cs remains in the post-evaporate simulant. While the crystal material exhibited some Cs, this is likely residual from the vacuum drying process of the crystals. Cs was not observed in the microscopy analysis of the material.

4. The solid material that was analyzed by XRD was quantified as majority natrophosphate, with small amounts of other materials as well. It is possible that there are other minor products that the XRD was not able to observe due to small quantities present.

5. The solids analyzed on the SEM showed a variety of different structures and morphologies. Plate-like structures were identified in regions as well as interspersed rod structures. Decreasing magnification illustrated thick, stacked plates with fibrous looking material. The birefringent nature of the materials is further indicative of natrophosphate.

5.4 Year 2 Efforts

Phosphate and fluoride processing studies will be performed with retrieval solutions generated from Task 2 year 1 efforts. Leachate solutions from AN-101 and AN-106 sludge segments will be comprehensively characterized and assed for Cs removal by batch contact tests using CST. A simulant will be developed based on the leachate composition found and ion exchange tests will be conducted to determine the potential for fluoride precipitation and to incorporate the complex anion composition effects on Cs exchange from the actual waste matrices. Additional ion exchange testing at multiple temperatures and/or dilutions may be conducted on wash water simulants based on evolving needs. If ample actual waste leachate solution is available, the solution will be evaporated to determine the resulting precipitant and compared to the simulant studies from year 1. Additionally, high gibbsite leachate from sludge segment AW-105 (generated from Task 2 year 1 efforts) will assess the equilibrium and ion exchange performance to compare to simulant studies from year 1.

6.0 References

Bolling, SD, JG Reynolds, TM Ely, JS Lachut, ME Lamothe, and GA Cooke. 2020. "Natrophosphate and kogarkoite precipitated from alkaline nuclear waste at Hanford." Journal of Radioanalytical and Nuclear Chemistry 323 (1): 329-339. https://doi.org/10.1007/s10967-019-06924-9.

Bray LA, KJ Carson, RJ Elovich. 1993. *Initial Evaluation of Sandia National Laboratory-Prepared Crystalline Silicotitanates for Cesium Recovery*. PNL-8847, Pacific Northwest Laboratory, Richland, Washington.

Fiskum SK, AM Rovira, JR Allred, HA Colburn, MR Smoot, AM Carney, TT Trang-Le, MG Cantaloub, EC Buck, and RA Peterson. 2019a. *Cesium Removal from Tank Waste Simulants Using Crystalline Silicotitanate at 12% and 100% TSCR Bed Heights*. PNNL-28527, Rev. 0; RPT-TCT-001, Rev. 0. Pacific Northwest National Laboratory, Richland, Washington.

Fiskum SK, AM Rovira, HA Colburn, AM Carney, and RA Peterson. 2019b. *Cesium Ion Exchange Testing Using a Three-Column System with Crystalline Silicotitanate and Hanford Tank Waste 241-AP-107*. PNNL-28958, Rev. 0; RPT-DFTP-013, Rev. 0. Pacific Northwest National Laboratory, Richland, Washington.

Herting, DL, GA Cooke, JS Page, and JL Valerio. 2015. Hanford Tank Waste Particle Atlas. Hanford Site (HNF), Richland, WA (United States) (United States). https://www.osti.gov/biblio/1423895

Hamm LL, T Hang, DJ McCabe, and WD King. 2002. *Preliminary Ion Exchange Modeling for Removal of Cesium from Hanford Waste Using Hydrous Crystalline Silicotitanate Material*. WSRC-TR-2001-00400; SRT-RPP-2001-00134. Westinghouse Savannah River Company, Aiken, South Carolina.

Hougan OA and WR Marshall, Jr. 1947. “Adsorption from a Fluid Stream Flowing Through a Stationary Granular Bed.” *Chemical Engineering Progress* 43(4):197-208.

Klinkenberg A. 1994. “Numerical Evaluation of Equations Describing Transient Heat and Mass Transfer in Packed Solids.” *Industrial and Engineering Chemistry* 40(10):1992.

Russell, RL, L Snow, and RA Peterson. 2010. "Methods to Avoid Post-Filtration Precipitation in Treatment of High-Level Waste." Separation Science and Technology 45 (12-13): 1814-1821. https://doi.org/10.1080/01496395.2010.493806.

Westesen AM, SK Fiskum, TT Trang-Le, AM Carney, RA Peterson. 2020. *Small to Full Height Scale Comparisons of Cesium Ion Exchange Performance with Crystalline Silicotitanate*. PNNL-30142, RPT-DFTP-019 Rev. 0, Pacific Northwest National Laboratory. Richland, Washington.

Westesen AM, AM Robb, NL Cappella, C Alvarez and RA Peterson. 2023. *Phosphate and Fluoride Processing Options for Hanford Sludge.* PNNL-34456 Rev. 0; APD-DFTP-001, Rev. 0. Pacific Northwest National Laboratory, Richland, Washington.

Westesen AM, AM Carney, EL Campbell, and RA Peterson. 2024. *Maximum Cs-137 Curie Loading onto Crystalline Silicotitanate for the Documented Safety Analysis of the Tank Side*

Cesium Removal Platform. PNNL-36241 Rev. 0; DFTP-RPT-042, Rev. 0. Pacific Northwest National Laboratory, Richland, Washington.

Wilmarth WR, VH Dukes, JT Mills and FF Fondeur 2000. Effect of Sodium Hydroxide Pretreatment of UOP IONSIV IE-911 Crystalline Silicotitanate Sorbent. WSRC-TR-2000-00167, Westinghouse Savannah River Company, Aiken, SC.

Appendix A – Column Load Data

The AN-107 lead, lag, and polish column loading raw data are provided in Table A.1. The raw data include the processed bed volumes (BVs) and corresponding ^{137}Cs concentration in the collected sample, % C/C_0, and the Cs decontamination factor (DF).

Table A.1. Lead and Lag Column Cs Breakthrough Results with 5.5 M Na Al Simulant

Lead Column				Lag Column			
BV	µCi ^{137}Cs/ mL	% C/C_0	DF	BV	µCi ^{137}Cs/ mL	% C/C_0	DF
10.8	2.51E-6	1.94E-1	5.16E+2	38.6	1.56E-6	1.21E-1	8.26E+2
38.6	5.92E-7	4.58E-2	2.18E+3	142.1	1.00E-6	7.78E-2	1.29E+3
92.6	3.48E-7	2.69E-2	3.71E+3	239.5	3.32E-7	2.57E-2	3.89E+3
142.1	3.43E-7	2.66E-2	3.76E+3	323.5	1.07E-6	8.32E-2	1.20E+3
187.4	3.52E-7	2.72E-2	3.67E+3	365.8	1.51E-7	1.17E-2	8.57E+3
239.4	2.76E-6	2.14E-1	4.68E+2	413.7	4.33E-7	3.35E-2	2.98E+3
288.1	1.89E-6	1.47E-1	6.82E+2	459.6	3.43E-7	2.66E-2	3.76E+3
365.8	4.96E-6	3.84E-1	2.60E+2	502.4	3.93E-7	3.04E-2	3.29E+3
413.8	8.73E-6	6.76E-1	1.48E+2	556.7	3.65E-7	2.83E-2	3.54E+3
502.5	1.87E-5	1.45E+0	6.91E+1	607.6	3.42E-7	2.65E-2	3.78E+3
607.7	4.46E-5	3.45E+0	2.90E+1	637.5	3.14E-7	2.43E-2	4.11E+3
637.4	5.00E-5	3.87E+0	2.59E+1				

BV = bed volume, 6 mL/BV
DF = decontamination factor
C_0 = 1.29E-03 µCi ^{137}Cs/ mL (reference date June 2024)

Appendix B – Batch Contact Results

Table B.1 provides the experimental results used to produce the Cs distribution coefficient (K_d) curves and isotherms for the four PO_4 and F simulants tested (Section 4.2.1 and 4.2.2 in the main body of this report). The dry crystalline silicotitanate (CST) masses were based on an F-factor of 0.934 at the nominal 105 °C drying temperature.

Table B.1. PO_4 and F Simulant Isotherm Data

Sample ID	Dry CST Mass (g)	AN-107 Vol. (mL)	Initial Cs Conc. (µg/mL)	Equil. Cs Conc. (M)	K_d (mL/g)	Q (mmoles Cs/g)
0.5 M Na Avg PO4/F Sim						
CST-0.5-S1	0.0747	15.0082	4.4	3.06E-07	21272	6.57E-03
CST-0.5-S1d	0.0747	14.4767	4.4	2.43E-07	25995	6.35E-03
CST-0.5-S2	0.0743	14.9528	16.8	1.20E-06	20633	2.51E-02
CST-0.5-S2d	0.0750	14.6155	16.8	1.02E-06	23667	2.44E-02
CST-0.5-S3	0.0751	14.9644	100.6	6.98E-06	21318	1.49E-01
CST-0.5-S3d	0.0744	14.4051	100.6	6.55E-06	21807	1.45E-01
CST-0.5-S4	0.0755	15.0342	2048.0	1.03E-02	101	1.01E+00
CST-0.5-S4d	0.0754	14.0083	2048.0	9.34E-03	118	1.13E+00
1.0 M Na Avg PO4/F Sim						
CST-1-S1	0.0742	15.0610	4.4	5.97E-07	10844	6.54E-03
CST-1-S1d	0.0742	14.7847	4.4	5.59E-07	11409	6.42E-03
CST-1-S2	0.0749	14.9928	16.5	2.85E-06	8538	2.43E-02
CST-1-S2d	0.0749	14.9676	16.5	5.51E-06	4237	2.37E-02
CST-1-S3	0.0752	14.9698	90.0	1.43E-05	9053	1.32E-01
CST-1-S3d	0.0753	14.8492	90.0	1.43E-05	9224	1.31E-01
CST-1-S4	0.0754	15.0693	2002.9	1.12E-02	70	7.80E-01
CST-1-S4d	0.0748	14.5550	2002.9	1.08E-02	75	8.25E-01
2.0 M Na Avg PO4/F Sim						
CST-2-S1	0.0744	15.0440	4.3	1.28E-06	4916	6.32E-03
CST-2-S1d	0.0743	14.8994	4.3	1.37E-06	4517	6.25E-03
CST-2-S2	0.0747	15.0076	16.6	5.51E-06	4405	2.39E-02
CST-2-S2d	0.0747	14.9193	16.6	5.16E-06	4689	2.39E-02
CST-2-S3	0.0745	14.9883	89.3	2.76E-05	4673	1.30E-01
CST-2-S3d	0.0743	14.9101	89.3	2.51E-05	5090	1.30E-01
CST-2-S4	0.0744	14.9825	1998.8	1.03E-02	91	9.45E-01
CST-2-S4d	0.0742	14.6773	1998.8	1.08E-02	79	8.43E-01
3.0 M Na Avg PO4/F Sim						
CST-3-S1	0.0752	15.0511	4.4	2.29E-06	2663	6.14E-03
CST-3-S1d	0.0741	14.1454	4.4	2.09E-06	2805	5.90E-03
CST-3-S2	0.0755	15.0567	16.5	8.33E-06	2734	2.30E-02
CST-3-S2d	0.0742	14.8385	16.5	8.46E-06	2686	2.31E-02
CST-3-S3	0.0744	15.0644	89.3	4.69E-05	2724	1.27E-01
CST-3-S3d	0.0747	14.8719	89.3	4.04E-05	3143	1.26E-01
CST-3-S4	0.0748	14.9699	1953.8	1.07E-02	74	7.94E-01
CST-3-S4d	0.0754	14.8725	1953.8	1.05E-02	76	8.24E-01
3.0 M Na Avg PO4/F Sim						
CST-3.8-S1	0.0751	15.0631	4.4	2.84E-06	2093	6.04E-03
CST-3.8-S1d	0.0744	14.8405	4.4	2.96E-06	2003	5.98E-03
CST-3.8-S2	0.0752	15.0051	16.5	1.23E-05	1784	2.23E-02
CST-3.8-S2d	0.0746	14.9195	16.5	1.18E-05	1881	2.24E-02
CST-3.8-S3	0.0750	15.0714	88.8	5.76E-05	2123	1.23E-01
CST-3.8-S3d	0.0744	14.9413	88.8	5.38E-05	2260	1.23E-01
CST-3.8-S4	0.0751	14.9594	1956.4	1.11E-02	64	7.26E-01
CST-3.8-S4d	0.0743	14.6260	1956.4	1.06E-02	77	8.19E-01

3.8 M Na High PO4/Low F Sim						
CST-P-S1	0.0752	14.7405	4.3	2.01E-06	2999	6.02E-03
CST-P-S1d	0.0746	14.7716	4.3	2.14E-06	2843	6.06E-03
CST-P-S2	0.0746	14.7763	17.0	8.31E-06	2862	2.37E-02
CST-P-S2d	0.0745	14.8128	17.0	8.51E-06	2786	2.38E-02
CST-P-S3	0.0753	14.7621	103.5	4.77E-05	3017	1.43E-01
CST-P-S3d	0.0753	14.7718	103.5	4.71E-05	3053	1.43E-01
CST-P-S4	0.0746	14.7951	2023.7	1.04E-02	92	9.58E-01
CST-P-S4d	0.0751	14.7820	2023.7	1.03E-02	94	9.70E-01
3.8 M Na Low PO4/High F Sim						
CST-F-S1	0.0752	14.9296	4.2	1.95E-06	3035	5.89E-03
CST-F-S1d	0.0753	14.9612	4.2	1.93E-06	3075	5.90E-03
CST-F-S2	0.0751	14.9392	16.9	7.52E-06	3155	2.38E-02
CST-F-S2d	0.0749	14.9443	16.9	8.80E-06	2683	2.36E-02
CST-F-S3	0.0745	14.9401	102.5	5.03E-05	2904	1.45E-01
CST-F-S3d	0.0751	14.9347	102.5	4.79E-05	3019	1.44E-01
CST-F-S4	0.0751	14.9644	2000.6	1.06E-02	83	8.81E-01
CST-F-S4d	0.0751	14.9512	2000.6	1.09E-02	77	8.35E-01
1.9 M Na Washed Sim						
CST-W-S1	0.0751	14.8585	4.3	9.33E-07	6607	6.17E-03
CST-W-S1d	0.0753	14.8540	4.3	9.09E-07	6783	6.15E-03
CST-W-S2	0.0748	14.8723	16.9	3.63E-06	6751	2.45E-02
CST-W-S2d	0.0753	14.8640	16.9	3.58E-06	6808	2.43E-02
CST-W-S3	0.0751	14.8668	103.4	2.18E-05	6870	1.50E-01
CST-W-S3d	0.0750	14.9010	103.4	2.34E-05	6413	1.50E-01
CST-W-S4	0.0750	14.9341	2022.3	1.04E-02	93	9.63E-01
CST-W-S4d	0.0750	14.9171	2022.3	1.04E-02	94	9.67E-01

Appendix C – Post Evaporation Loss Analysis

Evaporation mass losses were calculated for the five simulant matrices and are presented in Appendix C.

Table C-1 Post Evaporation Mass Loss in the Average PO_4^{3-}/F^- Simulant

Matrix ID	Phase	Ion	Starting Mass, g	Final Mass, g	Percent Loss Relative to Starting Simulant	Mol Difference Relative to Starting Simulant
Average PO_4^{3-}/F^- Simulant	Post Evaporate Simulant	Al^+	3.5	3.9	-13.4%	0.01
		OH^-	--	--	--	--
		F^-	1.9	1.3	33.9%	0.03
		Cl^-	2.4	2.2	10.5%	0.01
		K^+	2.5	2.3	7.5%	4.8E-03
		NO_2^-	98.6	89.4	9.3%	0.20
		NO_3^-	87.6	81.0	7.5%	0.11
		PO_4^{3-}	10.2	4.2	59.2%	0.06
		CO_3^{2-}	13.2	12.0	9.3%	0.02
		Na^+	163.6	139.7	14.6%	1.04
	Off-Gas Condensate	Al^+	3.5	ND	ND	ND
		OH^-	--	--	--	--
		F^-	1.9	1.7E-03	99.9%	0.10
		Cl^-	2.4	7.1E-04	100.0%	0.07
		K^+	2.5	ND	ND	ND
		NO_2^-	98.6	ND	ND	ND
		NO_3^-	87.6	ND	ND	ND
		PO_4^{3-}	10.2	2.1E-02	99.8%	0.11
		CO_3^{2-}	13.2	ND	ND	ND
		Na^+	163.6	ND	ND	ND

Table C-2 Post Evaporation Mass Loss in the High PO_4^{3-}/Low F^- Simulant

Matrix ID	Phase	Ion	Starting Mass, g	Final Mass, g	Percent Loss Relative to Starting Simulant	Mol Difference Relative to Starting Simulant
High PO_4^{3-} /Low F^- Simulant	Post Evaporate Simulant	Al^+	0.6	0.5	17.2%	4.0E-03
		OH^-	--	--	--	--
		F^-	0.5	0.3	24.1%	0.01
		Cl^-	2.0	2.1	-5.0%	2.8E-03
		K^+	3.1	2.3	27.0%	0.02
		NO_2^-	88.8	84.5	4.8%	0.09
		NO_3^-	33.0	34.1	-3.2%	0.02
		PO_4^{3-}	23.4	14.7	37.3%	0.09
		CO_3^{2-}	21.8	17.0	21.9%	0.08
		Na^+	164.0	141.7	13.6%	0.97
	Off-Gas Condensate	Al^+	0.6	ND	ND	ND
		OH^-	--	--	--	--
		F^-	0.5	ND	ND	ND
		Cl^-	2.0	1.2E-03	100.0%	0.06
		K^+	3.1	ND	ND	ND
		NO_2^-	88.8	ND	ND	ND
		NO_3^-	33.0	ND	ND	ND
		PO_4^{3-}	23.4	ND	ND	ND
		CO_3^{2-}	21.8	ND	ND	ND
		Na^+	164.0	3.9E-05	100.0%	7.13

Table C-3 Post Evaporation Mass Loss in the Low PO_4^{3-}/High F^- Simulant

Matrix ID	Phase	Ion	Starting Mass, g	Final Mass, g	Percent Loss Relative to Starting Simulant	Mol Difference Relative to Starting Simulant
Low PO_4^{3-} /High F^- Simulant	Post Evaporate Simulant	Al^+	5.3	4.0	23.8%	0.05
		OH^-	--	--	--	--
		F^-	3.4	3.1	8.9%	0.02
		Cl^-	2.7	2.7	-0.9%	7.3E-04
		K^+	3.8	2.9	23.5%	0.02
		NO_2^-	88.2	81.2	7.9%	0.15
		NO_3^-	108.4	105.3	2.9%	0.05
		PO_4^{3-}	1.6	2.2	-37.3%	0.01
		CO_3^{2-}	15.4	12.6	17.9%	0.05
		Na^+	170.2	155.6	8.6%	0.64
	Off-Gas Condensate	Al^+	5.3	ND	ND	ND
		OH^-	--	--	ND	ND
		F^-	3.4	ND	ND	ND
		Cl^-	2.7	7.7E-04	100.0%	0.08
		K^+	3.8	ND	ND	ND
		NO_2^-	88.2	ND	ND	ND
		NO_3^-	108.4	ND	ND	ND
		PO_4^{3-}	1.6	ND	ND	ND
		CO_3^{2-}	15.4	ND	ND	ND
		Na^+	170.2	ND	ND	ND

Table C-4 Post Evaporation Mass Loss in the Average PO_4^{3-}/F^- with $CsNO_3$ Simulant

Matrix ID	Phase	Ion	Starting Mass, g	Final Mass, g	Percent Loss Relative to Starting Simulant	Mol Difference Relative to Starting Simulant
Average PO_4^{3-}/F^- with $CsNO_3$ Simulant	Post Evaporate Simulant	Al^+	4.8	4.4	8.5%	0.02
		OH^-	--	--	--	--
		F^-	2.0	1.3	33.5%	0.04
		Cl^-	2.3	2.2	1.4%	9.2E-04
		K^+	2.7	2.5	7.3%	5.0E-03
		NO_2^-	97.8	92.5	5.5%	0.12
		NO_3^-	87.8	84.9	3.3%	0.05
		PO_4^{3-}	10.1	3.8	62.5%	0.07
		CO_3^{2-}	13.3	12.7	4.7%	0.01
		$^{133}Cs^+$	9.82E-02	9.07E-02	7.7%	5.7E-05
		Na^+	177.0	152.8	13.7%	1.05
	Off-Gas Condensate	Al^+	4.8	ND	ND	ND
		OH^-	--	--	--	--
		F^-	2.0	ND	ND	ND
		Cl^-	2.3	1.0E-03	100.0%	0.06
		K^+	2.7	ND	ND	ND
		NO_2^-	97.8	ND	ND	ND
		NO_3^-	87.8	1.2E-03	100.0%	1.42
		PO_4^{3-}	10.1	ND	ND	ND
		CO_3^{2-}	13.3	ND	ND	ND
		$^{133}Cs^+$	9.82E-02	6.9E-06	100.0%	7.39E-04
		Na^+	177.0	1.7E-02	100.0%	7.70

Table C-5 Post Evaporation Mass Loss in the Average PO_4^{3-}/F^- with $CsNO_3$ and ^{137}Cs Simulant

Matrix ID	Phase	Ion	Starting Mass, g	Final Mass, g	Percent Loss Relative to Starting Simulant	Mol Difference Relative to Starting Simulant
Average PO_4^{3-}/F^- with $CsNO_3$ and ^{137}Cs Simulant	Post Evaporate Simulant	Al^+	4.2	4.2	0.5%	8.0E-04
		OH^-	--	--	--	--
		F^-	2.0	1.2	36.7%	0.04
		Cl^-	2.3	1.9	15.4%	0.01
		K^+	2.5	2.4	4.3%	2.8E-03
		NO_2^-	97.6	95.9	1.7%	0.04
		NO_3^-	87.6	83.3	4.9%	0.07
		PO_4^{3-}	10.1	2.9	71.6%	0.08
		CO_3^{2-}	13.2	13.5	-2.1%	4.7E-03
		$^{137}Cs^+$	1.0E-07	9.0E-08	10.7%	8.1E-11
		Na^+	158.6	156.3	1.5%	0.10
	Off-Gas Condensate	Al^+	4.2			
		OH^-	--			
		F^-	2.0			
		Cl^-	2.3			
		K^+	2.5		ND	
		NO_2^-	97.6			
		NO_3^-	87.6			
		PO_4^{3-}	10.1			
		CO_3^{2-}	13.2			
		^{137}Cs	1.0E-07	Less than detection		--
		Na^+	158.6		ND	

Appendix D – X-Ray Diffraction

X-ray diffraction patterns were collected on the crystal materials from four of the simulant matrices. The low PO_4^{3-}/high F^- did not produce enough usable crystal material to obtain a diffraction pattern.

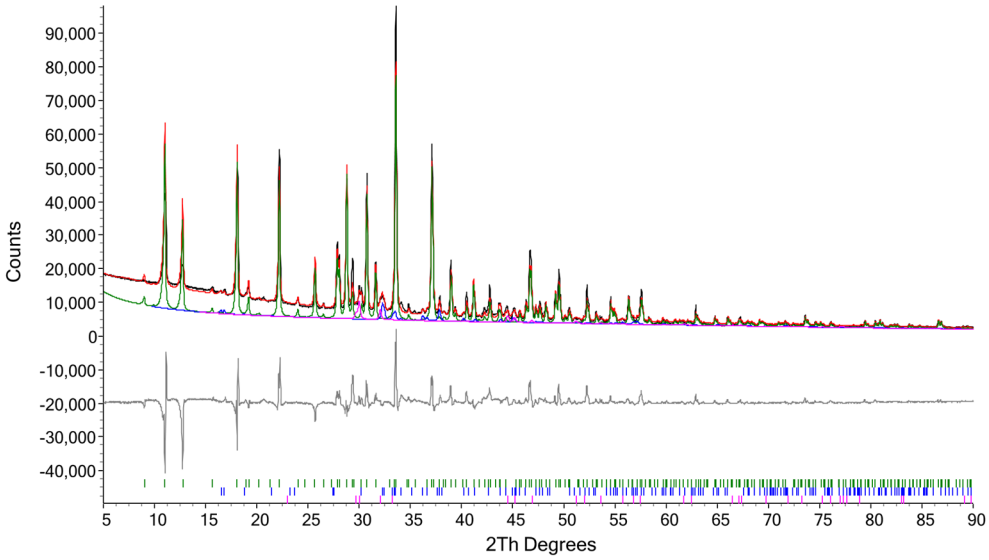

Figure D-1 Diffraction Pattern Collected for the Average PO_4^{3-}/F^- Simulant. (Black is the diffraction pattern, green is the fit of $Na_7FPO_4 \cdot 19H_2O$, blue is the fit of $Na_2CO_3 \cdot H_2O$, pink is the fit of $NaNO_2$, and the overall fit is red. Differences between the overall fit and the observed fit is in gray).

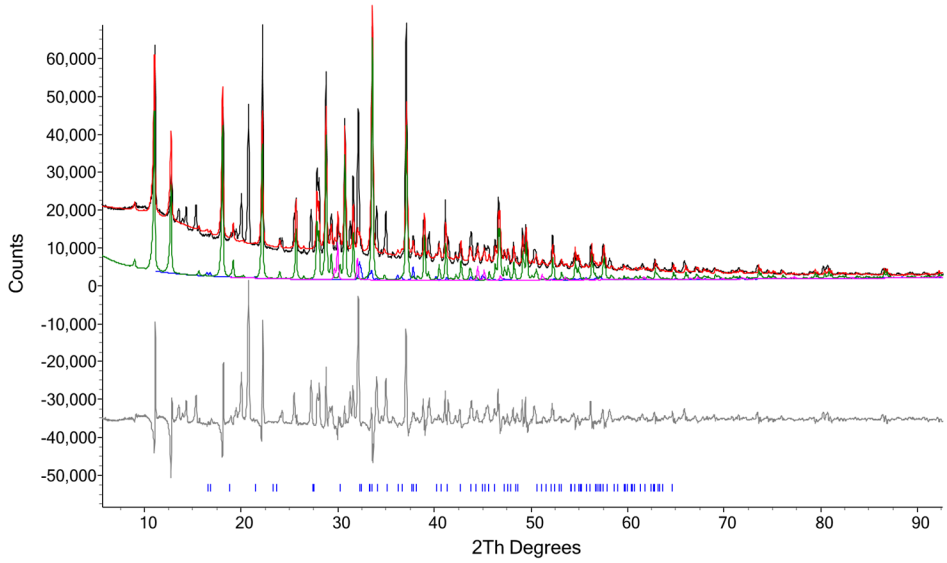

Figure D-2 Diffraction Pattern Collected for the High PO_4^{3-}/Low F^- Simulant. (Black is the diffraction pattern, green is the fit of $Na_7FPO_4 \cdot 19H_2O$, blue is the fit of $Na_2CO_3 \cdot H_2O$, pink is the fit of $NaNO_2$, and the overall fit is red. Differences between the overall fit and the observed fit is in gray.)

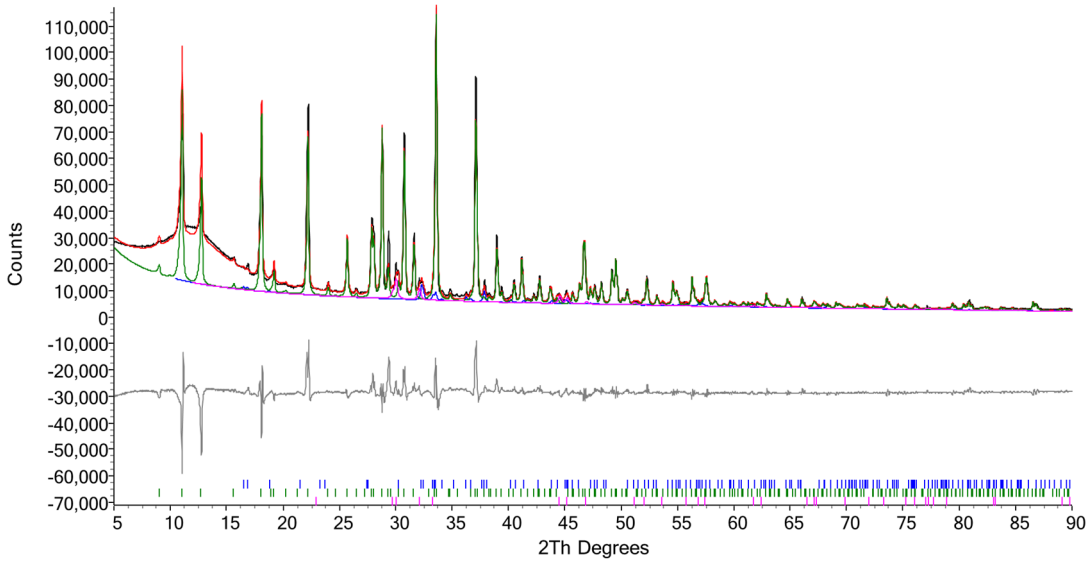

Figure D-3 Diffraction Pattern Collected for the Average PO_4^{3-}/F^- with $CsNO_3$ Simulant. (Black is the diffraction pattern, green is the fit of $Na_7FPO_4 \cdot 19H_2O$, blue is the fit of $Na_2CO_3 \cdot H_2O$, pink is the fit of $NaNO_2$, and the overall fit is red. Differences between the overall fit and the observed fit is in gray.)

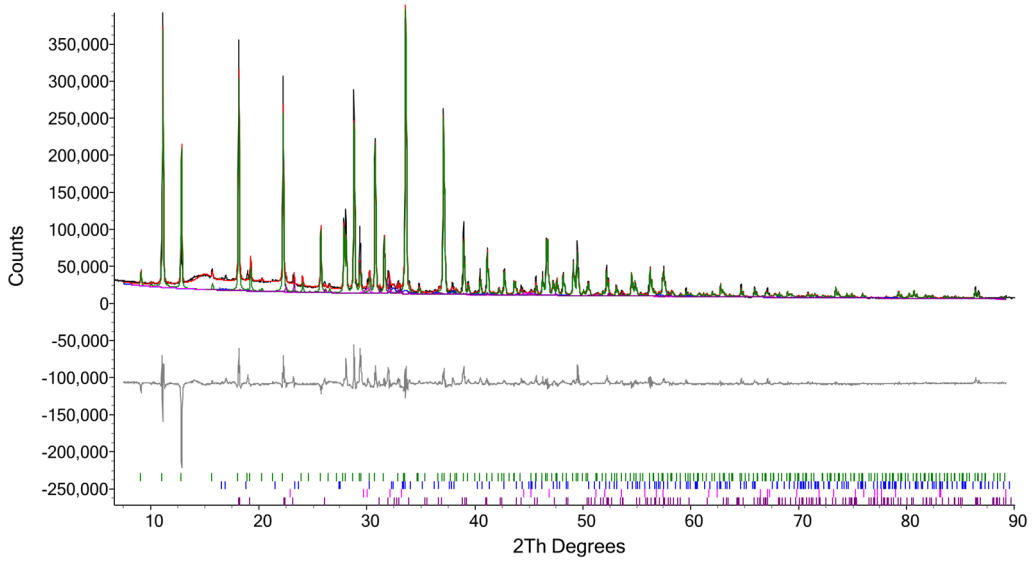

Figure D-4 Diffraction Pattern Collected for the Average PO_4^{3-}/F^- with $CsNO_3$ and ^{137}Cs Simulant. (Black is the diffraction pattern, green is the fit of $Na_7FPO_4 \cdot 19H_2O$, blue is the fit of $Na_2CO_3 \cdot H_2O$, pink is the fit of $NaNO_2$, purple is the fit of Na_2HPO_4, and the overall fit is red. Differences between the overall fit and the observed fit is in gray.)

Pacific Northwest National Laboratory

902 Battelle Boulevard
P.O. Box 999
Richland, WA 99354

1-888-375-PNNL (7665)

www.pnnl.gov